Insights into HO_X and RO_X chemistry in the boreal forest via measurement of peroxyacetic acid, peroxyacetic nitric anhydride (PAN) and hydrogen peroxide

John N. Crowley[1], Nicolas Pouvesle[1], Gavin J. Phillips[1], Raoul Axinte[1], Horst Fischer[1], Tuukka Petäjä[2], Anke Nölscher[1], Jonathan Williams[1], Korbinian Hens[1], Hartwig Harder,[1] Monica Martinez-Harder[1], Anna Novelli[1], Dagmar Kubistin[1], Birger Bohn[3], and Jos Lelieveld[1].

[1]Division of Atmospheric Chemistry, Max-Planck-Institute für Chemie, Mainz, Germany
[2]Institute for Atmospheric and Earth System Research INAR / Physics, University of Helsinki, Finland
[3]Forschungszentrum Juelich GmbH, 52425 Juelich, Germany

Correspondence to: John N. Crowley (john.crowley@mpic.de)

Abstract. Unlike many oxidised atmospheric trace gases, which have numerous production pathways, peroxyacetic acid (PAA) and PAN are formed almost exclusively in gas-phase reactions involving the hydroperoxy radical (HO_2), the acetyl peroxy radical ($CH_3C(O)O_2$) and NO_2 and are not believed to be directly emitted in significant amounts by vegetation. As the self-reaction of HO_2 is the main photochemical route to hydrogen peroxide (H_2O_2), simultaneous observation of PAA, PAN and H_2O_2 can provide insight into the HO_2 budget. We present an analysis of observations taken during a summertime campaign in a boreal forest that, in addition to natural conditions, was temporarily impacted by two biomass burning plumes. The observations were analysed using an expression based on a steady-state assumption using relative PAA-to-PAN mixing ratios to derive HO_2 concentrations. The steady-state approach generated HO_2 concentrations that were generally in reasonable agreement with measurements but sometimes overestimated those observed by factors of two or more. We also used a chemically simple, constrained box-model to analyse the formation and reaction of radicals that define the observed mixing ratios of PAA, H_2O_2. After nudging the simulation towards observations by adding extra, photochemical sources of HO_2 and $CH_3C(O)O_2$, the box model replicated the observations of PAA, H_2O_2, ROOH and OH throughout the campaign, including the biomass-burning influenced episodes during which significantly higher levels of many oxidized trace gases were observed. A dominant fraction of CH_3O_2 radical generation was found to arise via reactions of the $CH_3C(O)O_2$ radical. The model indicates that organic peroxy radicals were present at night in high concentrations that sometimes exceeded those predicted for daytime and initially divergent measured and modelled HO_2 concentrations and daily concentration profiles are reconciled when organic peroxy radicals are detected (as HO_2) at an efficiency of 35%. Organic peroxy radicals are found to play an important role in the recycling of OH radicals subsequent to their loss via reactions with volatile organic compounds.

1 Introduction

Peroxyacetyl nitric anhydride ($CH_3C(O)O_2NO_2$), commonly and hereafter referred to as PAN), plays a centrally important role as a reservoir of reactive nitrogen and transportation medium for NO_X from polluted to NO_X-poor regions of the atmosphere and thus impacts global tropospheric O_3 formation (Singh and Hanst, 1981; Fairlie et al., 2007; Zhang et al., 2008). This, combined with its influence on ecosystem health and productivity (Sparks et al., 2003) have made PAN a target of environmental research for several decades (Singh, 1987; Roberts, 1990; Grosjean, 2003). PAN is formed exclusively in the termolecular reaction of NO_2 with the peroxyacetyl radical (PA, $CH_3C(O)O_2$), which is considered one of the four most abundant organic peroxy radicals in the atmosphere (Tyndall et al., 2001).

PAN is thermally unstable, with a lifetime for re-dissociation to reactants (R-1) which is of the order of hours at temperatures close to 20 °C, but which increases to weeks or longer at lower temperatures as found e.g. at higher altitudes.

$$CH_3C(O)O_2 + NO_2 + M \qquad \rightarrow CH_3C(O)O_2NO_2 + M \qquad\qquad (R1)$$

$$CH_3C(O)O_2NO_2 + M \qquad \rightarrow CH_3C(O)O_2 + NO_2 + M \qquad\qquad (R-1)$$

As PAN is formed in reactions involving NO_2 and radicals formed from oxidation of organics its occurrence is frequently associated with photochemical ozone formation and PAN measurements have been interpreted to derive regional O_3 formation rates (Williams et al., 1997).

Peroxyacetic acid ($CH_3C(O)OOH$, hereafter PAA) is formed in a branch of the reaction of $CH_3C(O)O_2$ with HO_2 (R2) and is thus linked to PAN via their common organic, peroxy precursor radical.

$$CH_3C(O)O_2 + HO_2 \qquad \rightarrow CH_3C(O)OOH + O_2 \qquad\qquad (R2a)$$

$$\rightarrow CH_3C(O)OH + O_3 \qquad\qquad (R2b)$$

$$\rightarrow OH + CH_3CO_2 + O_2 \qquad\qquad (R2c)$$
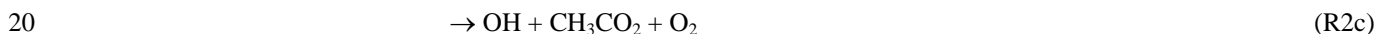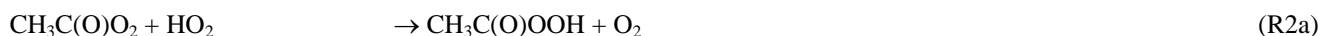
The fate of the CH_3CO_2 radical formed in (R2c) is decomposition to CO_2 and CH_3, the latter being converted immediately to CH_3O_2 in the presence of O_2.

Several recent experimental studies of reaction (R2) (Hasson et al., 2004; Dillon and Crowley, 2008; Jenkin et al., 2010; Groß et al., 2014) have shown that the dominant pathway (R2c) results in OH formation, contributing to HO_X recycling in NO_X poor regions (Lelieveld et al., 2008; Taraborrelli et al., 2012). The IUPAC preferred values for this reaction (Atkinson et al., 2006; IUPAC, 2018) are an overall rate coefficient at room temperature of $(2.2 \pm 0.4) \times 10^{-11}$ cm^3 molecule^{-1} s^{-1} with 50% ($\pm$ 10%) of reactive collisions resulting in OH formation (R2c) and branching ratios of 0.37 ± 0.1 and 0.13 ± 0.1 for R2a and R2b, respectively.

Under conditions of temperature and pressure found in the lowermost troposphere, the rate coefficients for reaction of $CH_3C(O)O_2$ with NO_2 and HO_2 are similar (k_1 at 298 K and 1 bar pressure is 9.3 x 10^{-12} cm^3 molecule^{-1} s^{-1}) and the relative flux of $CH_3C(O)O_2$ radicals into PAN and PAA formation will depend on the relative abundance of NO_2 and HO_2. Apart from extremely clean environments or very aged air pollution, when HO_2 concentrations approach those of NO_2, this will generally favour PAN. In the summertime boundary layer at mid-latitudes, PAN is however short lived and will readily

decompose back to $NO_2 + CH_3C(O)O_2$, implying that the formation of the thermally stable peroxy-acid in (R2a) will be a significant $CH_3C(O)O_2$ and HO_X sink in warm conditions with low NO_X levels.

Unlike PAN, there are few measurements of PAA (Fels and Junkermann, 1994; He et al., 2010; Zhang et al., 2010; Nguyen et al., 2015) and even fewer datasets in which PAN and PAA were both monitored (Zhang et al., 2010; Phillips et al., 2013).

5   A significant difference between PAA and many other organic acids is that, to the best of our knowledge, the former is generated in the gas-phase almost exclusively via reaction (R2a), whereas non-peroxy acids (e.g. its acetic acid co-product in R2b) may be emitted by vegetation (Talbot et al., 1995) or formed in reactions of O_3 with olefins (Grosjean, 1992) or by biomass burning (Talbot et al., 1988). PAA may also be formed in aerosols by the aqueous-phase oxidation of acetic acid by H_2O_2, but its high solubility and aqueous-phase equilibrium with $CH_3C(O)OH$ and H_2O preclude significant release into the

10   gas-phase.

Recently, we presented a dataset of quasi-simultaneous PAN and PAA measurements made at a boreal forest site in Finland (Phillips et al., 2013). In Phillips et al. (2013) more technical aspects of the measurement of PAN and PAA were described, though we also alluded to the fact that, due to their partly-common generation mechanism, PAN/PAA ratios may be a useful indicator of HO_2 levels. Here, we examine that aspect in more detail using an analytical expression that describes the PAA-

15   to-PAN ratio. We also combine the PAN and PAA measurements with those of several other trace gases and use chemical box-modelling with a highly simplified reaction scheme to gain insight into HO_X chemistry and the factors affecting PAN, PAA and H_2O_2 formation at the boreal site.

2 Campaign Site and Instruments

The HUMPPA-COPEC campaign in the summer of 2010 was located in the Finnish boreal forest at the SMEAR II-Hyytiälä

20   station (Hari and Kulmala, 2005) (Latitude 61º51ʹN; Longitude 24º17ʹE). The location of the site means that it experiences a very homogeneous fetch extending over hundreds of kilometres in all directions. A campaign overview with a list of instruments and an outline of the meteorological situation during the intensive (July and August) is given in Williams et al. (2011). The campaign period was unusually warm for this location (maximum temperature recorded was ~ 30 °C), mainly due to the above average contribution of air masses from the south, which resulted in enhanced biogenic emissions from the

25   forest and which also brought two episodes of biomass-burning impacted air to the site. The forest is dominated by a mixture of coniferous forest (Scots pine and Norway spruce) and mixed forest (conifers and silver birch). Most of the instruments from which data has been used in this work (PAN, PAA, H_2O_2, NO, NO_2, O_3 and HCHO) had inlets at the top of a ~20m high tower located in a small clearing (~20m diameter) in the forest and at approximately the same height as the surrounding tree-tops. Other data including OH and HO_2 and organic trace gases were taken by instruments located nearby (for details of

30   instrument positions and inlet heights see Williams et al 2011).

PAN and PAA were measured using an iodide chemical ionisation mass spectrometer (I-CIMS) as described in Phillips et al. (2013). Details of the instruments used to measure H_2O_2 and ROOH (enzyme / fluorescence), HCHO (Hantzch method),

NO$_X$ (chemiluminescence detector) organic peroxides and O$_3$ (UV) have been reported elsewhere (Stickler et al., 2006; Hosaynali Beygi et al., 2011; Fischer et al., 2015). Details of the OH-reactivity measurements and proton-transfer Mass Spectrometric (PTRMS) / GC measurements of organic trace gases have been previously given (Nölscher et al., 2012; Yassaa et al., 2012; Kourtchev et al., 2016). OH was measured by chemical ionisation mass spectrometry (Petäjä et al., 2009), HO$_2$ radicals were measured by laser induced fluorescence after conversion to OH as described in Hens et al. (2014) and Novelli et al. (2014). J-values were obtained from process specific parameterizations based on J-NO$_2$ and J-(O(^{1}D)) measured by filter radiometers (Bohn et al., 2008). Owing to known interferences by organic peroxy radicals (Fuchs et al., 2011; Fuchs et al., 2016; Lew et al., 2018), especially in forested regions, we refer to the measurements of HO$_2$ as "LIF-HO$_2$" which represent an upper limit to true HO$_2$ levels. Since discovery of this interference in 2010, it was eliminated from all later LIF measurements by reducing the amount of NO added internally to the sampled air and by regularly performing titration tests in the field.

3 Results and Discussion

Figure 1 displays measurements of PAN and PAA made by iodide-CIMS during HUMPPA-COPEC 2010 and several other trace gases (O$_3$, CO, H$_2$O$_2$, HCHO, NO$_X$) which provide some indication of the type of air masses sampled. Generally, the mixing ratios of PAN and PAA were similar, with PAN typically present at less than one ppb, reflecting the relatively low NO$_X$ levels (median, noon-time mixing ratio of 0.3 ± 0.1 ppbv) at this boreal forest site. In two campaign periods, day 207-211 and 219-221 highlighted in grey in Figure 1, elevated levels of PAN and especially PAA were observed, with mixing ratios of PAA exceeding 1 ppb compared to levels of less than 200 pptv during the rest of the campaign. These episodes of high PAA (and PAN) were accompanied by elevated mixing ratios of longer lived trace gases such as CH$_3$CN, CO, SO$_2$, HCHO and O$_3$, and were also coincident with higher than average temperatures. As discussed in Williams et al. (2011), CH$_3$CN measurements indicate that during these periods, the site was impacted by biomass burning in Russia, with back trajectories suggesting that the air from the fires had travelled for a few days before reaching the site.

An additional feature during the first episode (day 210.5) is a spike in the SO$_2$, HCHO and CO mixing ratios and also in non-oxidised hydrocarbons such as pentane (Williams et al., 2011). This shorter lived plume was associated with a continuous and rapid change in wind-direction (from ~25 to ~160 °) and higher local wind speeds (up to 25 km/hour), which resulted in arrival of biomass-burning impacted but less aged air masses to the site. The presence of sharply elevated SO$_2$ and pentane strongly suggests that fossil-fuel related emissions from St. Petersburg, (120°, 400 km distant), were mixed into this air mass, which may be regarded as chemically distinct from the other, longer-lasting biomass-burning episodes. NO$_X$ levels were not elevated during the biomass-burning plumes, confirming that they were chemically aged with respect to the conversion of NO$_X$ to NO$_Y$. Significant increases in signals at several PTRMS masses also indicated the presence of elevated amounts of oxygenated, volatile organic compounds (OVOCs, including organic acids, aldehydes and ketones) and also aromatic trace gases during the period where the site was impacted by the biomass burning plumes. The warmer

temperatures were also associated with increases in the emissions of biogenic trace gases (Paasonen et al., 2013; Kourtchev et al., 2016), making this a chemically very complex period during the campaign. An overview of several trace gases measured by the PTRMS is given in Figure S1 of the Supplementary Information.

5   Whilst the elevated levels of long lived biomass burning tracers such as CO and CH_3CN and biomass burning aerosol signal (Corrigan et al., 2013) are clearly due to long-range transport, this is unlikely to be the case for the shorter-lived trace gases. The very high OH-reactivity (up to 45 s^{-1}) observed (Nölscher et al., 2012) during the biomass-burning events and the fact that both H_2O_2 and PAA display diurnal profiles consistent with photochemical generation, suggest that the high levels of PAA, PAN and H_2O_2 are related to the presence of high levels of radical precursors in the biomass burning plumes, as

10 previously observed for boreal fires (Alvarado et al., 2010).

While PAA and PAN have similar photochemical generation routes, a cursory examination of their average diel profiles during the campaign (Figure 2) reveals important differences, with peak concentrations in the daily cycle of PAA displaced (later) relative to those of PAN by about 2 hours. This is related to the maximum loss rates of PAN (via thermal decomposition) which occur at the highest temperatures in the mid-afternoon. The day-to-day variations in the diel cycle of

15 PAA are mainly changes in the maximum mixing ratio, reflecting variable rates of production from precursors, with a nighttime concentration generally tending to zero. This is very similar to the diel profile of H_2O_2 which is also highly regular in shape and which, on most nights, also tends towards zero.

The mixing ratios of PAA are plotted against those of both H_2O_2 and PAN in Figure 3, which highlights the good correlation ($R^2 = 0.74$) with H_2O_2. The slope of the PAN to PAA ratio is reduced at high PAA mixing ratios, which were generally

20 observed when temperature and photochemical activity were highest. The more rapid loss of PAN at high temperatures causes the non-linear relationship and weakens the overall PAA to PAN correlation ($R^2 = 0.47$). The lower panel of Figure 3 indicates that PAA is strongly correlated with total organic peroxides (ROOH) and represents a significant fraction of total organic peroxides during the HUMPPA-COPEC campaign (Phillips et al., 2013). The PAN mixing ratios over the diel cycle were very variable, especially at nighttime.

25 Radiosondes suggest that for HUMPPA-COPEC-2010 the lowermost layer will be mixed with the residual layer by ≈ 10:00 local time (07:00 UTC), and we can consider the boundary layer thereafter to be mixed up to 1 km height with a further increase in BL height over the next two hours, depending on meteorological conditions (Ouwersloot et al., 2012). As rates of entrainment from the free troposphere and the vertical gradients of e.g. PAA are not known, in the subsequent analysis we assume that photochemical generation dominates the production side of the PAA budget but re-address this later when

30 comparing measured and model predictions of PAA and H_2O_2 mixing ratios.

Analysis of the net loss of PAN, O_3 and H_2O_2 during the pre-dawn period (midnight to 4 am, see Figure 2) by fitting exponential decay curves to the data during this period gives loss rate constants of 5.2×10^{-5} s^{-1} (H_2O_2), 2.3×10^{-5} s^{-1} (PAN) and 9.3×10^{-6} s^{-1} (O_3) resulting in campaign averaged, nighttime lifetimes of ≈ 7 hrs, 5hrs and 30 hrs, for H_2O_2, PAN and O_3, respectively. Note that as NO and HO_2 are absent or present in very low concentrations at night, the thermal decomposition

of PAN does not result in its efficient loss (see later). The night-time loss rates of H_2O_2, PAN and O_3 therefore reflect different rates of deposition to the canopy, although that of H_2O_2 will be a lower limit as nighttime production can occur via the ozonolysis of terpenes (see below).

The average, night-time loss rate constant for PAN of 2.3×10^{-5} s^{-1} can be equated to $2V_{ex}/h$ where V_{ex} is the exchange velocity and h is the boundary layer height (Shepson et al., 1992). This results in an approximate value of $V_{ex} \approx 0.23$ cm s^{-1} for an average, nighttime boundary layer height of 200 m for this campaign (Ouwersloot et al., 2012). This is consistent with values between 0 and 0.6 cm s^{-1} obtained at nighttime over coniferous forests (Shepson et al., 1992; Turnipseed et al., 2006; Wolfe et al., 2009). Wolfe et al. (2009) determined that the exchange velocity of PAN increased by a factor of ≈ 4 at noon compared to during the night, which is partially due to more efficient stomatal transport during the day. From this ratio, yielding an average, noon-time exchange velocity of ≈ 0.9 cm s^{-1} for HUMPPA-COPEC, and assuming a daytime boundary layer height of 1400m (Ouwersloot et al., 2012), we calculate noon-time loss rate constants for PAN deposition of $\approx 1 \times 10^{-5}$ s^{-1}. The high temperatures encountered during the summer in HUMPPA-COPEC-2010 campaign mean that daytime loss of PAN due to deposition is small compared to thermal dissociation followed by reaction of $CH_3C(O)O_2$ with NO or HO_2 (see below).

With a loss rate constant of 9.3×10^{-6} s^{-1}, the nighttime depletion of O_3 is slower than for PAN. From the values presented in Figure 2, the relative loss rate of O_3 and PAN is 0.4, which is similar to the value of 0.42 ± 0.19 reported e.g. by Shepson et al. (1992) and Wolfe et al. (2009), though such comparisons are complicated by variability in the chemical losses of O_3 via e.g. reaction with NO or sesquiterpenes (Kurpius and Goldstein, 2003) which depend on e.g. forest type, and emission rates.

The observed (net) loss rate constant for H_2O_2 is 5.2×10^{-5} s^{-1}, whereby ≈ 0.25 ppbv are lost in 4 hours between 00:00 and 04:00. The change in $[H_2O_2]$ results from a combination of its production via ozonolysis of terpenes and depositional losses. During the period from midnight to 04:00, the campaign average terpene and O_3 mixing ratios were 300 pptv and 38 ppbv, respectively. The five biogenic species measured by the GC (isoprene, α-pinene, myrcene, 3-carene and β-pinene) have rate constants for reaction with O_3 that vary between $\approx 1.3 \times 10^{-17}$ to 5×10^{-16} cm^3 molecule^{-1} s^{-1}. Taking into account the mean relative concentration and O_3-rate coefficient for each terpene, we derive an effective, campaign averaged rate constant of 1.5×10^{-16} cm^3 molecule^{-1} s^{-1} for the ozonolysis of terpenes. Taking a H_2O_2 yield of 0.16 (e.g. as observed for α-pinene) we calculate that ≈ 0.1 ppb H_2O_2 was generated during this period. Taken together with the observed (net) loss of H_2O_2, this implies a loss of 0.35 ppbv H_2O_2 by dry deposition in 4 hours, which translates to a loss rate constant of $\approx 8 \times 10^{-5}$ s^{-1}. Equating this value to $2V_{ex}/h$ (see above) we derive a nighttime deposition velocity for H_2O_2 of 0.8 cm s^{-1}. Given the assumptions made, the uncertainty related to this value is likely to be considerable. Nonetheless, the value obtained is entirely consistent with nighttime deposition velocities of 0.8 ± 0.2, 1.0 ± 0.3 and 1.6 ± 0.3 cm s^{-1} reported for H_2O_2 deposition over the Canadian boreal forest, with daytime H_2O_2 deposition velocities that are a factor 10 (± 5) larger (Hall and Claiborn, 1997). Using this factor we calculate daytime deposition velocities of 8 ± 4 cm s^{-1}. This can be equated to V_{ex}/h, which assumes no gradient in H_2O_2 in a well-mixed boundary layer. Taking into account the average daytime boundary layer

height of 1400 m during HUMPPA, this converts to a loss rate constant of $(6 \pm 3) \times 10^{-5}$ s^{-1} during the day. Later, we shall show that these values are consistent with results from the box-model based analysis of the dataset.

Hall and Claiborn (1997) measured deposition rates for summed organic peroxides (mainly CH$_3$OOH) which were a factor of about two-to-three lower than for H$_2$O$_2$ and Nguyen et al. (2015) measured deposition velocities for PAA over a temperate forest that were a factor two lower than H$_2$O$_2$. For our analysis, we apply daytime loss rates of ROOH, CH$_3$OOH and PAA due to deposition that are a factor two lower than for H$_2$O$_2$. In the following, we present a more detailed discussion of the chemical factors which control the relative abundance of PAA and PAN during the campaign.

3.1 Production and loss of PAN and CH$_3$C(O)OOH

In the absence of a sufficiently rapid reaction with OH ($k < 3 \times 10^{-14}$ cm^3 molecule^{-1} s^{-1}) and photo-dissociation (due to low cross sections and quantum yields in the tropospheric spectral range) (Talukdar et al., 1995), the lifetime of PAN during HUMPPA-COPEC-2010 was largely controlled by the temperature, which strongly affects its rate of thermal decomposition to CH$_3$C(O)O$_2$ and NO$_2$ (R-1). The relative concentrations of trace gases such as NO, and peroxy radicals (which can react with CH$_3$C(O)O$_2$ via R2 and R3) to that of NO$_2$ which regenerates PAN (R1) and its dry deposition rate d_{PAN} thus control its effective lifetime. Unlike other peroxides (e.g. H$_2$O$_2$) PAA is not formed at significant yield in the ozonolysis of BVOCs such as α-pinene (Li et al., 2016).

The most important reactions (R1, R-1, R2a) describing the formation and loss of PAN and PAA involve the acetyl peroxy radical (CH$_3$C(O)O$_2$) including its reaction with NO (R3).

$$\text{CH}_3\text{C(O)O}_2 + \text{NO} \; (+\text{O}_2) \qquad \rightarrow \text{CH}_3 + \text{CO}_2 \; + \text{NO}_2 \qquad\qquad\qquad \text{(R3)}$$

PAA will be lost by reaction with OH (R4)

$$\text{OH} + \text{CH}_3\text{C(O)OOH} \qquad \rightarrow \text{CH}_3\text{C(O)O}_2 + \text{H}_2\text{O} \qquad\qquad\qquad \text{(R4)}$$

By analogy with reactions of OH with H$_2$O$_2$ and CH$_3$OOH, Orlando and Tyndall estimated k_4 to be $\approx$ 1-5 $\times 10^{-12}$ cm^3 molecule^{-1} s^{-1} with CH$_3$C(O)O$_2$ (and H$_2$O) the predicted, dominant products following abstraction of the acidic H-atom in (R4) (Orlando and Tyndall, 2003). Theoretical work (Rypkema and Francisco, 2013) suggests that H-abstraction at the methyl group forming (in air) O$_2$CH$_2$C(O)OOH is also possible. Recent experimental work (Wu et al., 2017) suggests that k_4 may be as large as 1.1×10^{-11} cm^3 molecule^{-1} s^{-1} and this value has been adopted by the IUPAC panel (IUPAC, 2018) albeit with large associated uncertainty related to experimental difficulties.

The boundary layer lifetime of PAA and PAN will also be partially determined by deposition, especially in forests, as discussed above. The first-order rate constants representing dry deposition are d_{PAN} and d_{PAA}. Experimental work (Wu et al., 2015) on the uptake of PAA to ambient aerosol indicates an uptake coefficient (γ) of $\approx$ 3 $\times 10^{-4}$. Using the simplified expression (1) for the heterogeneous loss rate constant (k_{het}) of a trace gas to an aerosol particle:

$$k_{het} = 0.25\gamma\bar{c}A \qquad\qquad\qquad\qquad\qquad\qquad\qquad (1)$$

where $\bar{c} \approx 28000$ cm s^{-1} is the mean molecular velocity of PAA at room temperature and $A = 2 \times 10^{-6}$ cm^2 cm^{-3} is the aerosol surface area density results in an approximate loss rate constant of $\approx 5 \times 10^{-6}$ s^{-1} or a lifetime of about 3 days. Although PAA may be lost to aerosol in regions with extreme aerosol loading (Li et al., 2016) this loss term is negligible compared to e.g. depositional losses and reaction with OH in the boreal forest and is not considered further in this paper.

5   Considering only their in-situ, production and loss (i.e. ignoring advection) the net, relative rate of production of PAA and PAN (P_{PAA} and P_{PAN}, respectively) is given by:

$$\frac{P_{PAA}}{P_{PAN}} = \frac{k_{2a}[CH_3C(O)O_2]_{ss}[HO_2] - [PAA](k_4[OH] + d_{PAA})}{k_1[CH_3C(O)O_2]_{ss}[NO_2] - [PAN](k_{-1} + d_{PAN})} \tag{2}$$

where $[CH_3C(O)O_2]_{ss}$, is the steady state concentration of the acetylperoxy radical, determined by the ratio of its production and loss terms. On the right hand side of equation (2), the first terms of the numerator and denominator are readily

10   recognised as governing PAA and PAN production, whilst the second terms are the summed loss rates. If both PAA and PAN were to acquire steady state, their relative concentrations would be given by:

$$\frac{[PAA]}{[PAN]} = \frac{[HO_2]}{[NO_2]} \cdot \frac{k_{2a}(k_{-1} + d_{PAN})}{k_1(k_4[OH] + d_{PAA})} \tag{3}$$

Indicating that the PAA-to-PAN ratio depends on the relative abundance of HO$_2$ and NO$_2$. This is the expression we previously presented (Phillips et al., 2013) and which we used to derive very rough diel and campaign average HO$_2$ mixing

15   ratios of about 30 ppt.

$$[HO_2] = \frac{[PAA]}{[PAN]} \cdot [NO_2] \cdot \frac{k_1(k_4[OH] + d_{PAA})}{k_{2a}(k_{-1} + d_{PAN})} \tag{4}$$

Uncertainties of 30%, 25% and 15% for the mixing ratios of PAA, PAN and NO$_2$, respectively can be combined with uncertainties of 10-20% for the rate coefficients k_1, k_{2a} and k_{-1} and 50% uncertainty for the deposition velocities for PAA and PAN resulting in an overall uncertainty in [HO$_2$] of close to 75%.

20   Whether PAN and PAA acquire steady state (equivalence of production and loss terms in eqn. 2) depends on their loss rates. The first-order rate constant for PAN loss is given by the thermal decomposition rate constant (k_{-1}) multiplied by the fraction of the CH$_3$C(O)O$_2$ radical which does not reform PAN, plus the term for dry deposition, d_{PAN}, i.e.

$$\frac{-d[PAN]/dt}{[PAN]} = k_{-1} \cdot \frac{k_3[NO] + k_2[HO_2]}{k_3[NO] + k_2[HO_2] + k_1[NO_2]} + d_{PAN} \tag{5}$$

At a temperature of 298 K and at 1bar pressure, $k_1 = 8.7 \times 10^{-12}$ cm^3 molecule^{-1} s^{-1}, $k_{-1} = 3.8 \times 10^{-4}$ s^{-1} and $k_2 = k_3 \approx 2 \times 10^{-11}$

25   cm^3 molecule^{-1} s^{-1}. Using campaign average midday values of [NO$_2$] = 300 pptv, [NO] = 60 pptv and assuming [HO$_2$] = 20 pptv, we derive an effective PAN loss rate constant of 7.5×10^{-5} s^{-1} or a lifetime of $\approx$ 4 hours without considering deposition. The PAN lifetime will however vary greatly over the diel cycle and will increase substantially during colder, dark periods as the thermal dissociation slows down. In the absence of HO$_2$ and NO the dominant fate of the CH$_3$C(O)O$_2$ radical at night is to react with NO$_2$ to reform PAN. The lifetime of PAN through the campaign was calculated using the measured NO and

30   NO$_2$ concentrations and temperature and a model result for the HO$_2$ concentration (see section on box model below).
Time dependent values of d_{PAN} were derived using a sinusoidal variation of the boundary layer height during HUMPPA between ~1400 m during the day and ~200 m at night (Ouwersloot et al., 2012) which was matched in phase to the average

diel temperature variation during the campaign. Deposition of PAN was calculated with loss rate constants of 2.3×10^{-5} s^{-1} at night varying sinusiodally to a maximum value of 1.3×10^{-5} at 15:30 (see above). The lifetime for PAN throughout the campaign is displayed in Figure 4.

Similarly, the loss rate of PAA will be controlled by its reaction with OH multiplied by the fraction that does not reform

5   PAA (1-α), and its rate constant for dry deposition, d_{PAA}:

$$\frac{-d[PAA]/dt}{[PAA]} = k_4[OH] \cdot \frac{k_3[NO]+k_1[NO_2]+k_2(1-\alpha)[HO_2]}{k_3[NO]+k_1[NO_2]+k_2[HO_2]} + d_{PAA} \tag{6}$$

The second term on the right hand side of this expression varies between about 0.9 during the day and 1.0 at night when, to a first approximation, NO and HO_2 are very low. With the same conditions as given above, using a model result for the diel variation of the OH concentration and taking k_4 to be 1×10^{-11} cm^3 molecule^{-1} s^{-1} we derive an OH-induced PAA loss rate

10   constant of $\approx 1 \times 10^{-5}$ s^{-1}, or a lifetime greater than 10 hours. Thus, both dry deposition and reaction with OH determine the lifetime of PAA, though the dry deposition term dominates. The differences in the diel cycles of the PAA and PAN lifetimes are illustrated in Figure 4.

Use of a single, average boundary layer height and the same variation in exchange velocities for each day during the campaign means that the lifetime of PAA shows a very uniform behaviour, varying between ≈ 5 and 8 hours. In contrast,

15   noon-time PAN lifetimes are sometimes less than three hours, but increase up to 16 hours at night.

Bearing in mind that the long lifetimes of PAA and PAN may partially invalidate the assumption of steady state, we can insert noon-time values of PAA, PAN and NO_2 into expression (4) to derive HO_2 concentrations for each day during the campaign when data were available. The result is displayed in Figure 5, which also compares the HO_2 concentrations thus derived with direct measurements of LIF-HO_2 (Hens et al., 2014), available for only a limited period of the campaign.

20   The steady state calculations result in noon-time HO_2 concentrations between 5×10^8 and 2.5×10^9 molecule cm^{-3}.

On most days on which PAA, PAN and LIF-HO_2 data are available (209, 210, 214, 218), the agreement is reasonable, exceptions being days 211 and 217. Given that the PAA/PAN derived HO_2 concentrations are based on a steady state assumption and are heavily dependent on e.g. the PAA deposition rate, and the LIF-HO_2 data is likely to be an overestimate of HO_2 concentrations if high levels of organic peroxy radicals are present (Hens et al., 2014) the agreement may be

25   coincidental.

A further cause for the occasional disagreement, also related to the long lifetimes of PAN and PAA, may be the advection of NO_X from source that are too nearby for the PAN-to-PAA ratio to adapt and which will then result in an overestimation of HO_2 (see equation 4). Below, we compare the HO_2 concentrations derived from equation (4) with those from a photochemical box model and show that good agreement is found during the warmer periods of the campaign (when daytime

30   PAN lifetimes are shorter) but the disagreement can be significant during the colder periods when PAN is longer lived.

The HO_2 mixing ratio derived via equation (4) is rather insensitive to the rate coefficient for the reaction of OH with PAA, which is poorly constrained (IUPAC, 2018) or the concentration of OH if they lie within the expected ranges ($k_4 = 2\text{-}10 \times 10^{-12}$ cm^3 molecule^{-1} s^{-1}, and [OH] = $5\text{-}20 \times 10^5$ molecule cm^{-3}) reflecting the dominance of dry deposition losses of PAA such

that $d_{PAA} > k_6[OH]$. Likewise, at noon-time, the thermal decomposition rate of PAN is too rapid for the deposition term to impact on the calculation of HO$_2$ ($k_{-1} >> d_{PAN}$). The value of [HO$_2$] derived is however sensitive to the deposition rate of PAA chosen. An increase in d_{PAA} by a factor of two leads to a similar increase in [HO$_2$].

A more detailed insight into the chemical and meteorological factors controlling PAA and PAN can be gained from use of a time-dependent, photochemical box-model constrained by some of the longer lived trace gases that contribute centrally to local photochemical generation of radicals and thus PAA and PAN. This is described below.

3.2 Box Model Description

The box-model was developed with the goal of simulating the concentration of PAA and H$_2$O$_2$ over several diel cycles, which requires realistic diel variation in the photochemical production and loss rates of the CH$_3$C(O)O$_2$ and HO$_2$ radicals. A highly simplified approach was taken in which the diel variation of HO$_2$ and CH$_3$C(O)O$_2$ radical concentrations over periods of several days was constrained by measured (non-radical) trace gases and photolysis constants, but overall radical levels were adjusted to optimise the simulation of PAA and H$_2$O$_2$. This may be seen as complementary to the modelling exercise of Hens et al. (2014), who used a highly detailed chemical scheme and focussed on radical production in a bottom-up approach using a detailed reaction mechanism in which several biogenic organic trace gases were constrained.

In all model runs, the parameters directly constrained by observations were the temperature, concentrations of O$_3$, NO, NO$_2$, HONO, PAN, CO, HCHO, CH$_3$CHO, Σterpenes and the photolysis rate constants, J-O(^{1}D), J-NO$_2$, J-HONO, J-H$_2$O$_2$ and J-HCHO. The model CH$_4$ mixing ratio was held constant at 1.8 ppmv. In sensitivity runs, the concentrations of trace gases that were not measured (e.g. di-carbonyls, see later) were added to the model and their concentrations were calculated relative to those of related trace gases for which correlation is expected.

The complete reaction scheme is listed in Table S1 of the supplementary information. Rate coefficients were taken from the IUPAC evaluations (IUPAC, 2018). For the box-model, programmed in FACSIMILE code (Curtis and Sweetenham, 1987), several different scenarios were investigated, in which sections of the chemistry listed in Table S1 were deactivated or modified in order to investigate sensitivity of the model output (i.e. concentrations of PAA, H$_2$O$_2$, HO$_2$ and OH) to certain reactions and assumptions made, and to optimise the simulation of the measured concentrations of these trace gases and radicals. The box model simulated the field data at 10 min resolution. Due to the constraint (by measurements) of relatively long-lived trace gases such as O$_3$ and NO$_X$, the model acquired steady state in less than one day. The simulation was initiated at day 196, the output only used from day 202 to day 220 (for which PAA and PAN data were available). Essential features of the different model runs are listed in the section "box-model development" of the Supplementary information.

3.2.1 Model production and loss of HO$_X$ and ROx

OH was generated directly via O$_3$ photolysis, whereby the photolysis rate constant, J-O(^{1}D), was modified to take into account the relative rates of quenching of the O(^{1}D) atom by N$_2$ and O$_2$ and reaction with H$_2$O, i.e. it takes changes in

humidity throughout the campaign into account. OH was also generated by photolysis of H_2O_2 and HONO and via reaction of HO_2 with NO and O_3.

Loss of OH via reactions with the trace gases constrained by measurement such as CO, H_2O_2, HCHO, O_3 and NO_2 represent only a small fraction of the overall OH reactivity, which is dominated by organic trace gases (Nölscher et al., 2012). Thus,

5   two reactions in which OH was converted to organic peroxy radicals, were used to tune the model OH-reactivity and organic radical production rates. These OH-loss processes were parameterised as generic reactions of OH with biogenic trace gases and reactions with oxygenated volatile organic compounds (OVOCs) to form RO_2*. In this case RO_2* is distinct from the sum of organic peroxy radicals which is usually denoted RO_2. The mixing ratios of the biogenic trace gases (terpenoids) was constrained by PTR-MS measurements at high time resolution. The PTR-MS mixing ratios agreed with the summed

10   terpenoids from the GC measurements.

A generic rate constant of 7×10^{-11} cm^3 molecule^{-1} s^{-1} was used for the reaction of OH with terpenes. This was calculated from the relative concentrations of the terpenes as measured by GC and weighted with their individual rate constants for reaction with OH (Atkinson and Arey, 2003b; IUPAC, 2018).

The mixing ratios of OVOCs were linked by a factor (adjusted to obtain good agreement between observation and model

15   output) to measurements of CH_3CHO and HCHO: For the reaction of OVOC with OH we used a rate coefficient of 1×10^{-11} cm^3 molecule^{-1} s^{-1}. This approach is different to that taken by Hens et al. (2014) who tied missing OH-reactivity to an unknown trace gas that behaved like α-pinene but at concentrations that were a factor 5-10 higher than measured. Tying missing OH-reactivity to α-pinene could however not simulate the high OH-reactivities during the biomass burning impacted periods of the campaign.

20   The modelled OH-reactivity varied between 3 and 50 s^{-1}, the highest values being associated with the biomass-burning impacted days as observed. A comparison between modelled and measured OH-reactivity reveals broad agreement (Figure 6) with several high reactivity events captured by the model. The main exceptions are the events on day 202.5 (OH-reactivity up to 43 s^{-1}) and day 215 (peak OH-reactivity of 70 s^{-1}). Figure 6 also plots the time series of the organic content of aerosol, which varies in a similar manner to the modelled OH reactivity. This is expected as increased OH reactivity should lead to

25   larger rates of generation of condensable OVOCs and thus SOA mass. On the other hand, it will also reflect that the high values of OH reactivity are tied in the model to high levels of measured OVOCS (CH_3CHO and HCHO), which may also be correlated with organic aerosol content. The most prominent exceptions are again the very high OH reactivities at day 202.6 (~43 s^{-1}) and day 214.6 (~70 s^{-1}). No corroborative evidence for high reactivity on these days could be found in the extensive datasets available for this campaign. For example, there were no significant increases in any measured trace gases (biogenic

30   or biomass burning related), no reductions in the OH levels or enhanced formation of products such as HCHO. Instrument failure and subsequent tests resulted in an interruption in OH-reactivity measurements shortly before the sharp increase in OH-reactivity on day 214 was measured. Though it is not obvious why this should have resulted in such a large, positive bias

when measurements were resumed, the mismatch with other data, proximity to the power-down and exponential decay in the reactivity suggest that the instrument was not fully operational in this period.

RO_2^* reacted in the model with NO to form HO_2 (generic rate coefficient of 1×10^{-11} cm^3 molecule^{-1} s^{-1}) and with HO_2 to form peroxides (ROOH, with generic rate coefficient of 0.8×10^{-11} cm^3 molecule^{-1} s^{-1}) and regenerate OH at 0.2×10^{-11} cm^3

5   molecule^{-1} s^{-1}. As the chemical identity of the OVOCS are unknown a more explicit description of the chemistry was not warranted.

HO_2 was generated directly via photolysis of HCHO and from reactions of OH with O_3, CO, HCHO and H_2O_2, and the reaction of NO with CH_3O_2 and other peroxy radicals. The most important HO_2 reactions in the model are its self-reaction to form H_2O_2, and reaction with NO and O_3 to form OH. It also reacts with the $CH_3C(O)O_2$ radical (forming PAA and acetic

10   acid and recycling OH). The uptake of HO_2 to aerosol has been reported to be important for the HO_X budget under some conditions (Jacob, 2000; Liang et al., 2013). The present IUPAC evaluation (Ammann et al., 2013; IUPAC, 2018) for the heterogeneous interaction of HO_2 with aqueous aerosol has a dependence on the HO_2 concentration as well as the aerosol pH which is based on the formulation of Thornton et al. (2008). For average HUMPPA-COPEC conditions a value for the uptake coefficient (γ) between 10^{-3} and 10^{-4} is estimated. In combination with equation (2), and for $HO_2 = 5 \times 10^8$ molecule

15   cm^{-3} (≈ 20 pptv) this results in a loss rate for HO_2 of $\approx 1 \times 10^4 - 1 \times 10^5$ molecule cm^{-3} s^{-1}, which is insignificant compared to HO_2 loss rates via its self-reaction (1.5×10^6 molecule cm^{-3} s^{-1}) and reaction with NO (1.2×10^7 molecule cm^{-3} s^{-1} with NO = 100 pptv) close to midday. Heterogeneous losses of HO_2 were therefore not included in the model.

The rate of $CH_3C(O)O_2$ formation in the model is determined by the rate of oxidation or photolysis of its organic precursors, including the oxidation of CH_3CHO via reaction with OH:

20   OH + CH_3CHO + O_2 $\rightarrow$ $CH_3C(O)O_2$ + H_2O (R5)
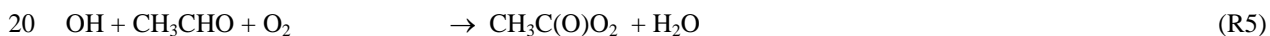
As we describe later, this reaction alone was not sufficient to describe the formation of PAA at the levels observed and the model was augmented with other $CH_3C(O)O_2$ sources such as the degradation of photo-labile carbonyl species. Tying $CH_3C(O)O_2$ production rates to the levels of oxidised VOCs as measured by the PTRMS was found to be especially important during biomass burning influenced periods in which VOCs (e.g. propane, butane) and OVOCs (e.g. CH_3CHO,

25    $CH_3C(O)OH$, CH_3OH) were also greatly enhanced.

Finally, in order to test potential radical sources leading to enhanced HO_X concentrations at nighttime, formation and reactions of the NO_3 radical were implemented in a simplified manner (See Table S1) as was the formation of OH via ozonolysis of alkenes.

3.2.2 Model production of H_2O_2 and PAA

30   PAN, PAA and H_2O_2 are NO_X dependent, stable products of HO_X, ROx and NO_X interactions. The goal of the modelling study is to examine whether their measurement can provide insight into the HO_X budget in the boreal environment by adapting a reaction scheme to match the observed mixing ratio of H_2O_2 and PAA over chemically different periods of the

campaign. H_2O_2 was generated in the model via the HO_2 self-reaction, the rate constant of which displays a complex dependence on temperature, pressure and humidity (IUPAC, 2018). The rate coefficient during the campaign varied between 4.3 and 7.2×10^{-12} cm^3 molecule^{-1} s^{-1}. We also include H_2O_2 formation from the ozonolysis of terpenes.

Model PAA was generated only in the reaction between HO_2 and $CH_3C(O)O_2$ radicals as described above. PAA and H_2O_2 may be lost via photolysis, reaction with OH, dry deposition and uptake to aerosol. As described in section (3.1) for PAA the first-order loss rate constant for heterogeneous reaction of H_2O_2 with aerosol particles can be calculated from expression (2) using $\bar{c} \approx 44000$ cm s^{-1}, $A = 2 \times 10^{-6}$ cm^2 cm^{-3} and $\gamma = 3 \times 10^{-4}$ (Wu et al., 2015), resulting in $k_{het} = 7 \times 10^{-6}$ s^{-1}. As concluded for PAA, loss of gas-phase H_2O_2 via uptake to aerosol is insignificant compared to dry deposition.

3.2.3 Dry Deposition

Depositional loss of PAA and H_2O_2 was simulated in the model using time dependent first order loss rate constants that were derived assuming a sinusoidal variation of the boundary layer height during HUMPPA between ~1400 m during the day and ~200 m at night (Ouwersloot et al., 2012) which was matched in phase to the average, diel temperature during the campaign. Deposition rate constants were calculated from deposition velocities from the literature scaled to the observed loss rate of PAA and H_2O_2 at night (see section 3). For H_2O_2, the data of Hall and Claiborn (1997) were used. Their values are chosen as they are expected to be most relevant for the Boreal tree type and forested environment but are still in broad agreement with other datasets for H_2O_2 deposition (Stickler et al., 2007). Following Nguyen et al. (2015), the daytime deposition of PAA was modelled to be 50% that of H_2O_2, with the same variation over the diel cycle. The diel cycle of the deposition velocities for PAA and H_2O_2 are displayed in Figure S2 of the Supplementary Information.

3.3 Box Model Results

The constrained model, with the photochemical sources of radicals described in section 3.2.1 significantly underestimated the observations of H_2O_2 and PAA, especially during the biomass burning episodes. Addition of an extra source of $CH_3C(O)O_2$ in the reaction of OH with OVOC (at 30% branching ratio) was found not to help as even small increases (less than factor of two) in the modelled concentration of PAA could only be achieved at the cost of reducing the OH, HO_2 and thus H_2O_2 concentrations significantly below the measurements. This is readily understood as PAA is an effective sink of HO_X for this low NO_X environment.

The PAA production rate was therefore enhanced by introducing a $CH_3C(O)O_2$ production term that does not require initiation by reaction with OH, i.e. photolysis of a precursor trace gas, which results in CH_3CO release. Acetone ($CH_3C(O)CH_3$) was present at mixing ratios of up to 10 ppbv during the periods impacted by biomass burning, yet its slow photolysis (lifetime of months) means that it is not a significant source of $CH_3C(O)O_2$ in the boundary layer. In contrast, dicarbonyls such as methyl-glyoxal ($CH_3C(O)CHO$), pyruvic acid ($CH_3C(O)C(O)OH$) or biacetyl ($CH_3C(O)C(O)CH_3$) have absorption spectra that extend beyond 400 nm, are rapidly photolysed and may represent an efficient source of $CH_3C(O)O_2$ and HO_2 if present at sufficient concentrations.

$$CH_3C(O)CHO + h\nu\ (O_2) \quad\quad \rightarrow CH_3C(O)O_2 + HO_2 + CO \quad\quad\quad\quad\quad (R6)$$

$$CH_3C(O)C(O)CH_3 + h\nu\ (O_2) \quad\quad \rightarrow 2\ CH_3C(O)O_2 \quad\quad\quad\quad\quad\quad\quad (R7)$$

$$CH_3C(O)C(O)OH + h\nu\ (O_2) \quad\quad \rightarrow CH_3C(O)O_2 + HO_2 + CO_2 \quad\quad\quad\quad (R8)$$
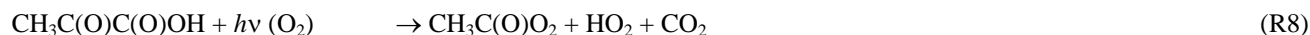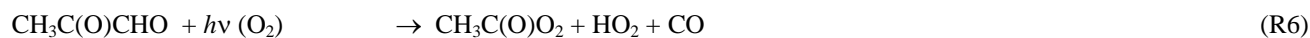
Addition of short-lived hydrocarbons including methyl-glyoxal has been found to increase $CH_3C(O)O_2$ radical production

5 rates in models of biomass burning plumes (Fischer et al., 2013) and to dramatically increase PAN production rates in a global model (Ito et al., 2007).

Methyl-glyoxal is formed at high yield from the OH-initiated oxidation of several biogenic (especially isoprene) and anthropogenic VOCs e.g. via degradation of aromatic hydrocarbons (Arey et al., 2009; Obermeyer et al., 2009) and is found in biomass burning impacted air masses (Fu et al., 2008; Akagi et al., 2011; Stockwell et al., 2015) and those influenced by

10 urban emissions of aromatics (Liu et al., 2010). It is also formed at yields of a several percent from the ozonolysis of mono-terpenes such as α-pinene and Δ^3-carene (Yu et al., 1998; Fick et al., 2003), which were both present at high concentrations during HUMPPA-COPEC-2010. Model estimates of PAN formation suggest that, on a global scale, 30% of the acetyl peroxy radical generation is the result of methyl-glyoxal degradation, with 44% arising via CH_3CHO oxidation by OH (Fischer et al., 2013).

15 Biacetyl is formed in the photo-oxidation of aromatic hydrocarbons in the presence of NO_X (Atkinson et al., 1980; Arey et al., 2009; Obermeyer et al., 2009) and is also expected to be present in biomass-burning impacted air-masses. The proposed intermediacy of dicarbonyls such as methyl-glyoxal and biacetyl in forming PAA in this study is consistent with the dominant role for di- and tri-alkyl benzenes in PAA formation found by Zhang et al. (2010). Pyruvic acid is formed in the gas-phase degradation of biogenic and anthropogenic hydrocarbons and has been observed at mixing ratios of hundreds of

20 pptv (Andreae et al., 1987; Jacob and Wofsy, 1988; Talbot et al., 1995; Veres et al., 2011). As a precursor in the biosynthesis of terpenoids, pyruvic acid can be directly emitted by vegetation resulting in very large mixing ratios (several ppbv) in a non-oxidative environment (Jardine et al., 2010). It is also found in secondary organic aerosol and may be formed in the aqueous phase reaction of methyl-glyoxal (Tan et al., 2012). In a recent campaign (IBAIRN, 2016) at the Hyytiälä site, our Iodide-CIMS instrument monitored large signals at $m/z = 87$, which we assigned to the $CH_3C(O)CO_2^-$ ion from pyruvic acid.

25 Post-campaign calibration of the CIMS resulted in mixing ratios of several hundred pptv, which were correlated with other biogenic trace gases. We thus have direct evidence of pyruvic acid at this site, albeit in the autumn (when emissions are likely to be weaker) rather than in the summer.

A further, short lived di-carbonyl that is formed in the OH and O_3-initiated degradation of several VOCs including alkenes, acetylene and aromatics (Calvert et al., 2000; Volkamer et al., 2001; Calvert et al., 2002) and which is present in biomass

30 burning (Fu et al., 2008) is glyoxal (HC(O)C(O)H). It is also formed at high yield (via glycol aldehyde) in the OH oxidation of methyl butenol (Atkinson and Arey, 2003a), emitted by pine trees and therefore of relevance for the HUMPPA-COPEC campaign. The photolysis of glyoxal is efficient (lifetimes at noon of ~ 4 hrs) and results in formation of two HO_2 radicals:

$$HC(O)CHO + h\nu\ (O_2) \quad\quad \rightarrow 2\ HO_2 + 2\ CO \quad\quad\quad\quad\quad\quad\quad\quad (R9)$$

In the absence of direct measurements, indications of the presence of biacetyl and methyl-glyoxal were sought in the PTR-MS dataset. Strong increases in mixing ratio at $m/z = 73$ and $m/z = 87$ were observed which would correspond to protonated methyl-glyoxal and biacetyl, respectively. Indeed, most PTR-MS masses monitored displayed similar trends, with strong increases during the biomass burning impacted periods. Campaign time series for selected masses are shown in the supplementary information (Figure S1).

For $m/z = 73$ a peak mixing ratio of ≈ 0.8 ppbv was observed during the first biomass burning event (day 206-212). At the same time a peak value of 0.5 ppbv was reported for mass 87. The PTRMS signal at mass 73 is usually considered to be methyl ethyl ketone (de Gouw and Warneke, 2007; Blake et al., 2009; Yanez-Serrano et al., 2016), a product of butane degradation. n-butane was enhanced during the biomass burning periods and correlated with $m/z = 73$, so that a significant (or dominant) contribution of methyl ethyl ketone to this mass is probable.

The PTRMS mass 87 (peaking at mixing ratios of 0.5 ppb during the biomass burning impacted periods) is usually assigned to 2-methyl-3-buten-2-ol (MBO) which is emitted from coniferous trees (Schade et al., 2000) but may have contribution from several trace gases including C5-carbonyls, butadione and methacrylic acid (de Gouw and Warneke, 2007; Blake et al., 2009; Muller et al., 2016). We are not aware that biacetyl has been reported at this mass.

Previous measurements of methyl-glyoxal and glyoxal in rural locations have revealed mixing ratios up to a few hundred pptv (see Fu, 2008 for a summary) which were correlated with those of HCHO (Lee et al., 1995) or CO (Spaulding et al., 2003) and which had mixed biogenic and anthropogenic sources. Greatly elevated concentrations of methyl-glyoxal (>900 pptv) and glyoxal (> 500 pptv.) have been observed in biomass burning impacted air masses in a rural environment (Kawamura et al., 2013). Even at sub 100 pptv levels, methyl-glyoxal was found to contribute significantly to $CH_3C(O)O_2$ radical production (Lee et al., 1995). We note that the PTR-MS is insensitive to glyoxal due to instability of the protonated parent-ion at $m/z = 59$ (Stoenner et al., 2017) which is dominated by acetone.

The potential impact of dicarbonyls on the HO_X and $CH_3C(O)O_2$ budget was investigated by incorporating methyl-glyoxal, biacetyl, glyoxal and pyruvic acid into the model with the concentrations of the first three di-carbonyls constrained by a correlation factor with CH_3CHO. Mixing ratios of pyruvic acid at this site (in autumn) have been found to be correlated with (and at similar concentration to) those of directly emitted biogenics and its concentration was arbitrarily set equal to that of the summed terpenes.

The ratios of CH_3CHO to methyl-glyoxal, biacetyl and glyoxal were varied to optimise the simulation of the measured PAA and H_2O_2 mixing ratios and resulted in maximum concentrations of methyl-glyoxal, glyoxal and biacetyl in the model of approximately 0.75, 0.15 and 1.3 ppbv, respectively, which were present during the peak of the biomass burning impacted episodes (when CH_3CHO levels were largest). The relative mixing ratios of di-carbonyls is not important for the model result, i.e. a reduction in the methyl-glyoxal mixing ratio would result in a decrease in both $CH_3C(O)O_2$ and HO_2 radical production, which could be balanced by an increase in pyruvic acid (with also generates one of each radical) or by an increase in both biacetyl and glyoxal, scaled by the relative J-values. Based on preferred experimental absorption spectra and quantum yields (IUPAC, 2018), the photolysis rates of pyruvic acid, glyoxal, methyl-glyoxal and biacetyl were modelled as

The incorporation of dicarbonyls into the model has the anticipated effect of increasing acetyl and HO$_2$ peroxy production rates and thus levels of PAA, especially during the biomass burning impacted periods. As seen in Figure 7, the model does a reasonable job of reproducing both PAA and H$_2$O$_2$. Especially encouraging is the good model-measurement agreement in the period between day 204 and 209, in which PAA levels increased by an order of magnitude and which were accompanied by

10   large increases in H$_2$O$_2$ and the generally good agreement with OH measurements. The measurement-model agreement is further exemplified in Figure 8 which plots the diel profiles of PAA and H$_2$O$_2$ and OH and the comparison with the model output for the same time period. Considering that we use a diel cycle for the deposition term that is unchanged for the whole campaign (i.e. does not vary with relative humidity, wind-speed, rates of turbulent mixing etc.) and thus does not reflect any variation in the meteorological situation at the site, the agreement for H$_2$O$_2$ and PAA is very good and, within the observed

15   variability and considering the experimental uncertainty in the measurements, the model captures the average variation of each trace gas across the diel cycle. It is also noteworthy, that the model captures the non-zero OH levels at nighttime as well as the noon-time maximum values. This contrasts with the conclusions of Hens et al. (2014), who also modelled the reaction of ozone with biogenics (but using speciated terpenes from GC-measurements) and were unable to generate and sustain sufficient OH at nighttime to match the observations. Although the difference may be partially related to our use of PTRMS

20   measured terpenes and an average yield of OH based on latest recommendations for individual terpenes, the main effect is the nighttime recycling of HO$_2$ and OH via reactions of peroxy radicals formed from OH generated in ozonolysis reactions. Given the high OH-reactivities measured during the HUMPPA-COPEC-2010 campaign, the fate of most OH radicals formed at nighttime will be reaction with terpenes and other VOCs to form RO$_2$*. At nighttime, in the absence of NO, the main fates of peroxy radicals are reaction with HO$_2$ and self-reaction. In the model, the reaction of RO$_2$* with HO$_2$ forms ROOH (80%)

25   with a minor (20%) reaction pathway forming OH as observed in laboratory studies (at yields of 10-60%) for several substituted oxidised organic peroxy radicals (Dillon and Crowley, 2008; Jenkin et al., 2010; Groß et al., 2014).

The self-reaction of RO$_2$* is modelled to form HO$_2$ (via the degradation of the alkoxy radicals formed in the first step) so that non-zero concentrations of, HO$_2$ and RO$_2$* are predicted to be present at night. The modelled, HO$_2$ and RO$_2$* concentrations are displayed in Figure 9a. The initially surprising result is that RO$_2$* radicals are present at night at

30   concentrations that are comparable to, or even exceed those predicted for the daytime. This reflects the weak sinks of RO$_2$* at nighttime (owing to the absence of NO), rather than high rates of production. The diel cycles of RO$_2$* (Figure 9d) and HO$_2$ (Figure 9c) are very different. Whereas the HO$_2$ concentration is defined by its photochemical production, with a maximum coinciding with the maximum of the actinic flux and low concentrations at night, that of RO$_2$* shows two distinct, broad maxima, one at noon and one at midnight, both at concentrations of $\approx 5 \times 10^8$ molecule cm^{-3} ($\approx$ 20 pptv). The modelled

RO$_2$*-to-HO$_2$ ratio is $\approx$ 1 at 12:00 UTC, increasing to $\approx$ 5 at midnight. This is consistent with the box-model result of Hens et al. (2014) who report RO$_2$-to-HO$_2$ ratios of between 0.5 and 4.5.

RO$_2$* production at night occurs via OH (formed via ozonolysis of alkenes and reaction of O$_3$ with HO$_2$) with OVOC and terpenes, the weak sinks enabling it to build up in concentration. The modelled, rapid depletion of RO$_2$* at sunrise is a result of increasing NO concentrations, which is followed by a second maximum in the RO$_2$* concentration at noon resulting from photochemical generation of OH. Organic radicals have previously been observed at nighttime in several locations and are often attributed to the O$_3$ initiated oxidation of organics (Hu and Stedman, 1995; Cantrell et al., 1997; Reiner et al., 1997; Salisbury et al., 2001; Geyer et al., 2003; Emmerson and Carslaw, 2009; Sommariva et al., 2011; Andrés-Hernández et al., 2013). Nighttime concentrations of ROx (HO$_2$ + RO$_2$ in molecule cm^{-3}) of 5-7 $\times$ 10^8 (Reiner et al., 1997), 1-2 $\times$ 10^9 (Andrés-Hernández et al., 2013), $\approx$ 2 $\times$ 10^8 (Geyer et al., 2003) and $\approx$ 4 $\times$ 10^8 (Hu and Stedman, 1995) have been reported, which are consistent with the model results discussed here, albeit for chemically different locations. The double maximum in RO$_2$* is also consistent with the data of Geyer et al. (2003) who observed a similar double maximum in ROx at noon and late evening.

Figure 7 indicates that the measured, midday values of LIF-HO$_2$ are generally larger than modelled HO$_2$ and that the diel variation in LIF-HO$_2$ (including large nighttime values) is incompatible with the modelled HO$_2$ profile (red line). LIF-HO$_2$ measurements as measured during HUMPPA-COPEC 2010 are prone to interference from organic peroxy radicals (Fuchs et al., 2011; Fuchs et al., 2016; Lew et al., 2018) and the predicted presence of large concentrations of RO$_2$* at nighttime has important consequences for our interpretation of the LIF-HO$_2$ data set. In Figure 9b, we plot the LIF-HO$_2$ concentrations along with modelled HO$_2$ with a fractional contribution from RO$_2$* (i.e. [HO$_2$]$_{model}$ + 0.35[RO$_2$]$_{model}$).

The result (red line) reproduces not only the high apparent nighttime values of HO$_2$ observed but also the non-linear dependence on actinic flux and the higher values during the episodes impacted by biomass burning. Assuming that the RO$_2$* are detected as HO$_2$ with an efficiency of 35% thus reconciles measurement and model results, and is consistent with detection efficiencies for longer chain organic peroxy radicals.

Figure 10 shows the modelled time-series of RO$_2$*, CH$_3$O$_2$ and CH$_3$C(O)O$_2$. The organic peroxy radicals formed from reaction of OH with OVOCs and terpenes (RO$_2$*) are most abundant, reflecting the fact that the OH reactivity in the model is dominated by these trace gases. CH$_3$O$_2$ is also present at high concentrations and Figure S3 of the supplementary information plots the time dependent reactive flux through each of the reactions in the model that generate it. The dominant reactions are those of the CH$_3$C(O)O$_2$ radical, which reacts via formation of CH$_3$C(O)O, which decarboxylates to form the CH$_3$ radical and thus (via O$_2$ addition) CH$_3$O$_2$. In comparison, the formation of CH$_3$O$_2$ via CH$_4$ oxidation represents, on average, less than 10% of the total.

Organic peroxides (ROOH) other than PAA are important indicators of coupling between organic peroxy radicals and HO$_2$. The smallest member of the ROOH family is CH$_3$OOH, formed in the reaction between CH$_3$O$_2$ and HO$_2$:

$$CH_3O_2 + HO_2 \rightarrow CH_3OOH + O_2 \tag{R10}$$
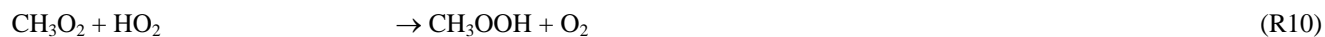
Larger ROOH are also formed via e.g. the OH initiated oxidation of VOCs (e.g. terpenes, $C_{10}H_{16}$) in air:

$$OH + C_{10}H_{16} (+ O_2) \qquad \rightarrow HOC_{10}H_{16}O_2 \qquad\qquad\qquad\qquad\qquad (R11)$$

$$HOC_{10}H_{16}O_2 + HO_2 \qquad \rightarrow HOC_{10}H_{16}OOH + O_2 \qquad\qquad\qquad\qquad (R12)$$

$$HOC_{10}H_{16}O_2 \qquad (+ O_2) \qquad \rightarrow HOM + OH \qquad\qquad\qquad\qquad\qquad (R13)$$
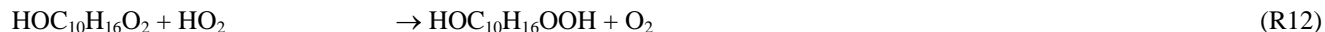
5 The conventional formation of ROOH, from reaction of the terpene derived peroxy radical via reaction with HO_2, may be augmented for some terpenes by auto-oxidation to also release OH and form a highly oxygenated molecule (HOM), that may partition substantially to the particle phase (Ehn et al., 2012).

Speciated organic peroxides were not measured during the campaign, but an indication of their levels was gained from the measurement of total organic peroxides (see section 2), which is biased towards those which are soluble and will thus have a

10 significant contribution from PAA. In Figure 11 we plot (red line) the model predicted time series of summed PAA and CH_3OOH mixing ratios after taking into account their known collection efficiencies in the scrubber (~90% for PAA, 60% for CH_3OOH). Model CH_3OOH is formed only in reaction (R10) and the sources of the CH_3O_2 precursor are limited to the reactions (R2c) and (R3), which both initially generate CH_3CO_2, which decomposes to CH_3 and thus CH_3O_2 in the presence of O_2 as well as (R14) and (R15):

15 $$OH + CH_4 (+ O_2) \qquad\qquad \rightarrow CH_3O_2 + H_2O \qquad\qquad\qquad\qquad\qquad (R14)$$

$$OH + CH_3OOH \qquad\qquad \rightarrow CH_3O_2 + H_2O \qquad\qquad\qquad\qquad\qquad (R15)$$

The removal of CH_3OOH in the model is mainly due to reaction with OH and dry deposition, the latter being set to 50% that of H_2O_2. Figure 11 reveals that the transition from low to high mixing ratios of CH_3OOH during the pre- and post-biomass burning periods is adequately reproduced in the model and, given the assumptions made above, agreement in terms of

20 absolute concentrations is also satisfactory. The blue line in Figure 11 was obtained by assuming that model derived ROOH is also detected but with a reduced efficiency of 0.1. The modelled sum of PAA and CH_3OOH is close to the measured sum of organic peroxides, indicating that these peroxides dominate the total organic peroxide measured by the instrument. Detection of other peroxides, even with low sensitivity (blue line), results in a model over-prediction. This likely reflects the fact that model generated ROOH are much less soluble than PAA or CH_3OOH and thus only a small fraction is detected.

25 Alternatively, peroxides with large, substituted organic groups (e.g. those formed from terpenes) are likely to partition to the aerosol phase.

Correlation diagrams (day 202 to 220) of measured versus modelled mixing ratios and concentrations of PAA, H_2O_2, ROOH, HO_2 and OH are displayed in Figure 12. The agreement between modelled and measured PAA, OH and H_2O_2 is generally good, with slopes that are, within the error limits of the measurements, equivalent to one. The exception is LIF-HO_2 (slope of

30 0.48) which is the result of an interference in the measurement as described above.

RO_2 radicals may also be formed at night in the NO_3 initiated oxidation of organics (Salisbury et al., 2001; Emmerson and Carslaw, 2009; Sommariva et al., 2011; Andrés-Hernández et al., 2013). NO_3 is formed via the reaction between NO_2 and O_3

and in forested areas, in the absence of strong, local NO emissions, will be lost mainly via reaction with unsaturated hydrocarbons such as terpenes forming nitrated peroxy radicals (N-RO$_2$)

$$NO_2 + O_3 \qquad\qquad \rightarrow NO_3 + O_2 \qquad\qquad\qquad\qquad\qquad (R16)$$

$$NO_3 + VOC\ (+ O_2) \qquad\qquad \rightarrow N\text{-}RO_2 \qquad\qquad\qquad\qquad\qquad (R17)$$

5 Like other peroxy radicals these can react with NO or NO$_3$ or HO$_2$ eventually forming a variety of multi-functional, organic nitrates (Ng et al., 2016). The reaction with NO proceeds via an alkoxy radical, which, via reaction with O$_2$, may also form HO$_2$. As HO$_2$ reacts with NO$_3$ to form OH radicals, NO$_3$ reactions can represent a nighttime source of HO$_X$ radicals (Platt et al., 1990). However, due to the high concentrations of terpenes measured during night in HUMPPA-COPEC-2010 the steady state concentration of NO$_3$ was reduced to less than one pptv (Rinne et al., 2012) so that reaction with HO$_2$ or RO$_2$ will be

10 reduced in importance. As PAN and thus CH$_3$C(O)O$_2$ are present at night, the reaction between HO$_2$ and CH$_3$C(O)O$_2$ is also an efficient route to OH (R2c). In both scenarios, NO$_3$ and CH$_3$C(O)O$_2$ can be considered to perform the same job as NO during the day: conversion of HO$_2$ to OH. Model NO$_3$ mixing ratios were less than 0.1 pptv, consistent with upper limits reported in previous NO$_3$ measurements at this site (Rinne et al., 2012; Liebmann et al., 2018). In agreement with Hens et al. (2014) we find that NO$_3$ reactions are an insignificant source of nighttime HO$_X$ and RO$_2$ during HUMPPA-COPEC-2010.

15 Our photochemical box-model does not explicitly take into account the effect of early morning entrainment of trace gases such as H$_2$O$_2$ and PAA from the residual layer. We have examined the potential effect of entraining H$_2$O$_2$ by simulating its down-mixing from higher (above canopy) levels that are likely to be richer in H$_2$O$_2$ due to the absence of dry deposition in air-masses disconnected from the ground. Entrainment of H$_2$O$_2$ from the residual layer would increase its canopy level mixing ratio in the morning when ground heating results in mixing of the PBL and the overlying layers. The point at which

20 entrainment starts each morning was defined by the time at which the trend in temperature at 16.8 m (close to canopy top) switched from negative to positive. This was usually between about 05:00 and 06:00 UTC, but variable owing to variable cloud cover. The concentration of H$_2$O$_2$ in the upper layers was taken to be same as that modelled for the previous afternoon at 16:00 when insolation weakens and the residual layer starts forming. The effect of entrainment was coded in the model by allowing a proxy for H$_2$O$_2$ (at the H$_2$O$_2$ concentration from the previous afternoon) to decay to form H$_2$O$_2$ at a constant rate

25 until the temperature at canopy top stopped increasing (usually over a period of $\approx$ 6 hours) and the boundary layer was well mixed. The effect of the modelled entrainment was to skew the diel profile of H$_2$O$_2$ to larger pre-noon values and away from the average trend observed. While it is clear that entrainment from higher layers can increase pre noon mixing ratios, it appears that this effect is much weaker than the photochemical formation of H$_2$O$_2$ during this campaign.

3.3.1 Model Sensitivity to PAA losses

30 Due to lack of experimental data, there is some uncertainty associated with the physical constants describing the main loss processes for PAA and the preferred value of the rate constant for its reaction with OH carries an uncertainty of a factor of two (IUPAC, 2018). The nighttime loss-rate constants for H$_2$O$_2$ and PAA were derived from measurements but the daytime values were scaled using literature data for H$_2$O$_2$ as described above. So far, we have adopted the results of Nguyen et al.

 In a sensitivity study, we reduced the daytime deposition velocity of PAA to just 25% that of H_2O_2. The nighttime value was held at the measured value. As expected, the modelled PAA mixing ratios increased with the model-to-measurement ratio also increasing from 0.86 to 1.09. Considering the total uncertainty of the PAA measurements, both results are however statistically indistinguishable from 1

5 and can be considered to be in satisfactory agreement.

The sensitivity of the model output to the OH-rate coefficient was tested by reducing it by a factor of two from the IUPAC recommended value of 1.1×10^{-11} cm^3 molecule^{-1} s^{-1}. This is the lower limit of the IUPAC recommendation and is close to previous estimates based on analogous reactions of OH with organic peroxides. As expected, a reduction in the loss term increased the modelled PAA mixing ratio, the model-to-measurement ratio also increasing slightly from 0.86 to 0.92. The

10 weak sensitivity to the OH + PAA rate coefficient in the range 5-11 $\times 10^{-12}$ cm^3 molecule^{-1} s^{-1} is expected as this reaction contributes only a small fraction of the overall loss of PAA, which is dominated by dry deposition. On the other hand, increasing the OH-rate coefficient to 2.2×10^{-11} cm^3 molecule^{-1} s^{-1} results in this reaction becoming competitive with dry deposition, with a reduction in the model-to-measurement ratio from 0.86 to 0.77.

3.3.2 Modelled sources of radicals during HUMPPA-COPEC-2010

15 Having constructed a photochemical chemical scheme that can 1) mimic the diel behaviour of several traces gases (PAA, H_2O_2 and, with some caveats, CH_3OOH) that are strongly linked to HO_2, and RO_2 concentrations, and 2) which can reproduce the measured concentrations of OH and HO_2, we can use the model to identify the relative contributions of the processes forming OH, HO_2 and $CH_3C(O)O_2$ during the campaign. The results are summarised as campaign averages (days 202-220) in Figure 13.

20 Fig. 13c indicates that the major source of the acetylperoxy radical in the model is the photolysis of the di-carbonyls biacetyl, methyl-glyoxal and pyruvic acid, together accounting for 61%, with almost all of the remaining $CH_3C(O)O_2$ coming from PAN decomposition. The reaction of CH_3CHO with OH accounted for only 4%.

For HO_2 (Fig. 13b) the picture is more complex with direct (primary) formation via the photolysis of formaldehyde, methyl-glyoxal and pyruvic acid accounting for 24%, the major source being the reaction between organic peroxy radicals and NO

25 (64%). This observation is consistent with the conclusions of (Kim et al., 2013) who required an extra source of HO_2 in their constrained model of HO_X chemistry in a MBO / terpene emitting environment. Kim et al. (2013) suggested photolysis of OVOCs as the missing source of HO_X, or that the RO_2 to HO_2 conversion is more efficient than modelled. Similar conclusions were drawn by Hens et al. (2014), who suggest that un-measured organic trace gases that are responsible for "missing" OH reactivity during HUMPPA-COPEC-2010 are a major source of HO_2. Hens et al. (2014) also found that

30 between 76 and 90% of HO_2 was formed by reactions of RO_2 with NO, depending on the reactivity of OH (lower values at lower OH-reactivity) in agreement with our conclusions that organic peroxy radical reactions with NO were the most important source of HO_2 during the campaign.

For OH, we find the main source to be the reaction of HO_2 with NO (47%), while direct formation from O_3 photolysis contributes on average only 7%. As the greatest contribution to HO_2 formation is from the reactions of organic peroxy radicals, which are formed mainly via OH + VOCs, this represents efficient HO_X re-cycling even in the low NO_X conditions of the boreal forest. This is in qualitative agreement with (Kim et al., 2013) who found that the reaction of HO_2 with NO is $\approx$

5   20 times as important as primary production of OH from O_3 photolysis in a non-isoprene forested environment with daytime NO levels close to 200 pptv. The results are also consistent with the box-modelling conclusions of Hens et al. (2014) who found the major source of OH to be reaction of HO_2 with NO and O_3 (73-80%) with only 20-27% generated directly (i.e. by photolysis of O_3, HONO and H_2O_2 and reaction of VOCs with O_3).

4 Conclusions

10   Simultaneous measurements of PAA, PAN and H_2O_2 were used to calculate HO_X levels during the HUMPPA-COPEC-2010 campaign in the boreal forest. A simple expression, based on the measured PAA-to-PAN ratio was used to calculate noon-time HO_2 mixing ratios during each campaign day. Good agreement with the model was found on some days, whereas on others the expression resulted in HO_2 levels that were a factor of two too high, which is likely related to varying degrees of breakdown of the inherent assumptions of PAA and PAN being in steady state at noon.

15   A box model, constrained by measurements of relatively long-lived radical precursors such as PAN, O_3, NO, NO_2, HCHO and CH_3CHO reproduced the observations of PAA, H_2O_2 and OH when extra, photolytic sources of HO_2 and $CH_3C(O)O_2$ were included (pyruvic acid, glyoxal, methyl-glyoxal and biacetyl). Inclusion of these radical sources was especially important during the biomass-burning influenced period when high levels of many oxygenated VOCs were observed. Measurements of HO_2, available for a limited number of days during the campaign, were generally higher (factor of two on

20   average) than those modelled. The model indicated large concentrations of organic peroxy radicals at nighttime and the apparent discrepancy between modelled and measured HO_2 could be resolved by considering the detection of RO_2 as HO_2 (with an efficiency of 35%) by the LIF-FAGE instrument during this campaign. Reactions involving organic peroxy radicals form a main HO_X recycling mechanism through the production of HO_2 radicals that subsequently react with NO and produce OH. Reactions of acetylperoxy radicals with HO_2 and NO were found to be the most important source of CH_3O_2 radicals.

25   An improved data analysis (both analytical and box-model) would require more accurate kinetic data on the reaction of PAA with OH and also on the temperature dependence of PAA formation in the reaction of $CH_3C(O)O_2$ with HO_2. Significant uncertainty is also associated with deposition velocities for PAA (in the steady-state analysis) and both PAA and H_2O_2 (in the box-model analysis). Future studies of HO_X chemistry in this type of environment would benefit greatly from measurements of vertical gradients (or deposition velocities) of PAA and H_2O_2 as well as measurements of speciated RO_2,

30   di-carbonyls and OVOCs.

References

Akagi, S. K., Yokelson, R. J., Wiedinmyer, C., Alvarado, M. J., Reid, J. S., Karl, T., Crounse, J. D., and Wennberg, P. O.: Emission factors for open and domestic biomass burning for use in atmospheric models, Atmos. Chem. Phys., 11, 4039-4072, doi:10.5194/acp-11-4039-2011, 2011.

Alvarado, M. J., Logan, J. A., Mao, J., Apel, E., Riemer, D., Blake, D., Cohen, R. C., Min, K. E., Perring, A. E., Browne, E. C., Wooldridge, P. J., Diskin, G. S., Sachse, G. W., Fuelberg, H., Sessions, W. R., Harrigan, D. L., Huey, G., Liao, J., Case-Hanks, A., Jimenez, J. L., Cubison, M. J., Vay, S. A., Weinheimer, A. J., Knapp, D. J., Montzka, D. D., Flocke, F. M., Pollack, I. B., Wennberg, P. O., Kurten, A., Crounse, J., St Clair, J. M., Wisthaler, A., Mikoviny, T., Yantosca, R. M., Carouge, C. C., and Le Sager, P.: Nitrogen oxides and PAN in plumes from boreal fires during ARCTAS-B and their impact on ozone: an integrated analysis of aircraft and satellite observations, Atmos. Chem. Phys., 10, 9739-9760, doi:10.5194/acp-10-9739-2010, 2010.

Ammann, M., Cox, R. A., Crowley, J. N., Jenkin, M. E., Mellouki, A., Rossi, M. J., Troe, J., and Wallington, T. J.: Evaluated kinetic and photochemical data for atmospheric chemistry: Volume VI – heterogeneous reactions with liquid substrates, Atmos. Chem. Phys., 13, 8045-8228, doi:10.5194/acp-13-8045-2013, 2013.

Andreae, M. O., Talbot, R. W., and Li, S. M.: Atmospheric measurements of pyruvic and formic acid, J. Geophys. Res. -Atmos., 92, 6635-6641, doi:10.1029/JD092iD06p06635, 1987.

Andrés-Hernández, M. D., Kartal, D., Crowley, J. N., Sinha, V., Regelin, E., Martínez-Harder, M., Nenakhov, V., Williams, J., Harder, H., Bozem, H., Song, W., Thieser, J., Tang, M. J., Hosaynali Beigi, Z., and Burrows, J. P.: Diel peroxy radicals in a semi-industrial coastal area: nighttime formation of free radicals, Atmos. Chem. Phys., 13, 5731-5749, doi:10.5194/acp-13-5731-2013, 2013.

Arey, J., Obermeyer, G., Aschmann, S. M., Chattopadhyay, S., Cusick, R. D., and Atkinson, R.: Dicarbonyl Products of the OH Radical-Initiated Reaction of a Series of Aromatic Hydrocarbons, Env. Sci. Tech., 43, 683-689, doi:10.1021/es8019098, 2009.

Atkinson, R., Carter, W. P. L., Darnall, K. R., Winer, A. M., and Pitts, J. N.: A smog chamber and modelling study of the gas-phase NOx-air photo-oxidation of toluene and the cresols, Int. J. Chem. Kinet., 12, 779-836, doi:10.1002/kin.550121102, 1980.

Atkinson, R., and Arey, J.: Gas-phase tropospheric chemistry of biogenic volatile organic compounds: a review, Atmos. Env., 37, S197-S219, 2003a.

Atkinson, R., and Arey, J.: Atmospheric degradation of volatile organic compounds, Chem. Rev., 103, 4605-4638, doi:10.1021/cr0206420, 2003b.

Atkinson, R., Baulch, D. L., Cox, R. A., Crowley, J. N., Hampson, R. F., Hynes, R. G., Jenkin, M. E., Rossi, M. J., and Troe, J.: Evaluated kinetic and photochemical data for atmospheric chemistry: Volume II - reactions of organic species, Atmos. Chem. Phys., 3625-4055, 2006.

Blake, R. S., Monks, P. S., and Ellis, A. M.: Proton-Transfer Reaction Mass Spectrometry, Chem. Rev., 109, 861-896, doi:10.1021/cr800364q, 2009.

Bohn, B., Corlett, G. K., Gillmann, M., Sanghavi, S., Stange, G., Tensing, E., Vrekoussis, M., Bloss, W. J., Clapp, L. J., Kortner, M., Dorn, H. P., Monks, P. S., Platt, U., Plass-Dulmer, C., Mihalopoulos, N., Heard, D. E., Clemitshaw, K. C., Meixner, F. X., Prevot, A. S. H., and Schmitt, R.: Photolysis frequency measurement techniques: results of a comparison within the ACCENT project, Atmos. Chem. Phys., 8, 5373-5391, 2008.

Burkholder, J. B., Sander, S. P., Abbatt, J., Barker, J. R., Huie, R. E., Kolb, C. E., Kurylo, M. J., Orkin, V. L., Wilmouth, D. M., and Wine, P. H.: Chemical Kinetics and Photochemical Data for Use in Atmospheric Studies, Evaluation No. 18," JPL Publication 15-10, Jet Propulsion Laboratory, Pasadena, http://jpldataeval.jpl.nasa.gov., 2015.

Calvert, J. G., Atkinson, R., Kerr, J. A., Madronich, S., Moortgat, G. K., Wallington, T. J., and Yarwood, G.: The Mechanisms of Atmospheric Oxidation of the Alkenes, Oxford Univ. Press, New York, 2000.

Calvert, J. G., Atkinson, R., Becker, K. H., Seinfeld, J. H., Wallington, T. J., and Yarwood, G.: The mechanism of atmospheric oxidation of aromatic hydrocarbons, Oxford University Press, New York, 2002.

Cantrell, C. A., Shetter, R. E., Calvert, J. G., Eisele, F. L., and Tanner, D. J.: Some considerations of the origin of nighttime peroxy radicals observed in MLOPEX 2c, J. Geophys. Res. -Atmos., 102, 15899-15913, 1997.

Corrigan, A. L., Russell, L. M., Takahama, S., Aijala, M., Ehn, M., Junninen, H., Rinne, J., Petaja, T., Kulmala, M., Vogel, A. L., Hoffmann, T., Ebben, C. J., Geiger, F. M., Chhabra, P., Seinfeld, J. H., Worsnop, D. R., Song, W., Auld, J., and Williams, J.: Biogenic and biomass burning organic aerosol in a boreal forest at Hyytiala, Finland, during HUMPPA-COPEC 2010, Atmos. Chem. Phys., 13, 12233-12256, 2013.

Curtis, A. R., and Sweetenham, W. P.: Facsimile, Atomic Energy Research Establishment, Report R-12805, 1987, 1987.

de Gouw, J., and Warneke, C.: Measurements of volatile organic compounds in the earths atmosphere using proton-transfer-reaction mass spectrometry, Mass Spectrom. Rev., 26, 223-257, doi:10.1002/mas.20119, 2007.

Dillon, T. J., and Crowley, J. N.: Direct detection of OH formation in the reactions of HO_2 with $CH_3C(O)O_2$ and other substituted peroxy radicals, Atmos. Chem. Phys., 8, 4877-4889, 2008.

Ehn, M., Kleist, E., Junninen, H., Petäjä, T., Lönn, G., Schobesberger, S., Dal Maso, M., Trimborn, A., Kulmala, M., Worsnop, D. R., Wahner, A., Wildt, J., and Mentel, T. F.: Gas phase formation of extremely oxidized pinene reaction products in chamber and ambient air, Atmos. Chem. Phys., 12, 5113-5127, doi:10.5194/acp-12-5113-2012, 2012.

Emmerson, K. M., and Carslaw, N.: Nighttime radical chemistry during the TORCH campaign, Atmos. Env., 43, 3220-3226, doi:10.1016/j.atmosenv.2009.03.042, 2009.

Fairlie, T. D., Jacob, D. J., and Park, R. J.: The impact of transpacific transport of mineral dust in the United States, Atmos. Env., 41, 1251-1266, doi:10.1016/j.atmosenv.2006.09.048, 2007.

Fels, M., and Junkermann, W.: The occurrence of organic peroxides in air at a mountain site, Geophys. Res. Lett., 21, 341-344, doi:10.1029/93gl01892, 1994.

Fick, J., Pommer, L., Nilsson, C., and Andersson, B.: Effect of OH radicals, relative humidity, and time on the composition of the products formed in the ozonolysis of alpha-pinene, Atmos. Env., 37, 4087-4096, doi:10.1016/s1352-2310(03)00522-3, 2003.

Fischer, E. V., Jacob, D. J., Yantosca, R. M., Sulprizio, M. P., Millet, D. B., Mao, J., Paulot, F., Singh, H. B., Roiger, A.-E., Ries, L., Talbot, R. W., Dzepina, K., and S, P. D.: Atmospheric peroxyacetyl nitrate (PAN):
a global budget and source attribution, Atmos. Chem. Phys. Discuss.,, 13, 26841–26891, 2013.

Fischer, H., Pozzer, A., Schmitt, T., Jockel, P., Klippel, T., Taraborrelli, D., and Lelieveld, J.: Hydrogen peroxide in the marine boundary layer over the South Atlantic during the OOMPH cruise in March 2007, Atmos. Chem. Phys., 15, 6971-6980, 2015.

Fu, T. M., Jacob, D. J., Wittrock, F., Burrows, J. P., Vrekoussis, M., and Henze, D. K.: Global budgets of atmospheric glyoxal and methylglyoxal, and implications for formation of secondary organic aerosols, J. Geophys. Res. -Atmos., 113, doi:10.1029/2007jd009505, 2008.

Fuchs, H., Bohn, B., Hofzumahaus, A., Holland, F., Lu, K. D., Nehr, S., Rohrer, F., and Wahner, A.: Detection of HO2 by laser-induced fluorescence: calibration and interferences from RO2 radicals, Atmos. Meas. Tech., 4, 1209-1225, 2011.

Fuchs, H., Tan, Z. F., Hofzumahaus, A., Broch, S., Dorn, H. P., Holland, F., Kunstler, C., Gomm, S., Rohrer, F., Schrade, S., Tillmann, R., and Wahner, A.: Investigation of potential interferences in the detection of atmospheric ROx radicals by laser-induced fluorescence under dark conditions, Atmos. Meas. Tech., 9, 1431-1447, 2016.

Geyer, A., Bachmann, K., Hofzumahaus, A., Holland, F., Konrad, S., Klupfel, T., Patz, H. W., Perner, D., Mihelcic, D., Schafer, H. J., Volz-Thomas, A., and Platt, U.: Nighttime formation of peroxy and hydroxyl radicals during the BERLIOZ campaign: Observations and modeling studies, J. Geophys. Res. -Atmos., 108, art. 8249, doi:10.1029/2001JD000656 2003.

Grosjean, D.: Formic acid and acetic acid- emissions, atmospheric formation and dry deposition at two southern California locations, Atmos. Env. A, 26, 3279-3286, doi:10.1016/0960-1686(92)90343-j, 1992.

Grosjean, D.: Ambient PAN and PPN in southern California from 1960 to the SCOS97-NARSTO, Atmos. Env., 37, S221-S238, doi:10.1016/s1352-2310(03)00392-3, 2003.

Groß, C. B. M., Dillon, T. J., Schuster, G., Lelieveld, J., and Crowley, J. N.: Direct kinetic study of OH and O_3 formation in the reaction of $CH_3C(O)O_2$ with HO_2, The Journal of Physical Chemistry A, 118, 974-985, doi:doi:10.1021/jp412380z, 2014.

Hall, B. D., and Claiborn, C. S.: Measurements of the dry deposition of peroxides to a Canadian boreal forest, Journal of Geophysical Research: Atmospheres, 102, 29343-29353, doi:10.1029/97jd01113, 1997.

Hari, P., and Kulmala, M.: Station for Measuring Ecosystem–Atmosphere Relations (SMEAR II), Boreal Env. Res., 10, 315–322, 2005.

Hasson, A. S., Tyndall, G. S., and Orlando, J. J.: A product yield study of the reaction of HO_2 radicals with ethyl peroxy ($C_2H_5O_2$), acetyl peroxy ($CH_3C(O)O_2$), and acetonyl peroxy ($CH_3C(O)CH_2O_2$) radicals, J. Phys. Chem. A, 108, 5979-5989, 2004.

He, S. Z., Chen, Z. M., Zhang, X., Zhao, Y., Huang, D. M., Zhao, J. N., Zhu, T., Hu, M., and Zeng, L. M.: Measurement of atmospheric hydrogen peroxide and organic peroxides in Beijing before and during the 2008 Olympic Games: Chemical and physical factors influencing their concentrations, J. Geophys. Res. -Atmos., 115, doi:D17307
10.1029/2009jd013544, 2010.

Hens, K., Novelli, A., Martinez, M., Auld, J., Axinte, R., Bohn, B., Fischer, H., Keronen, P., Kubistin, D., Nolscher, A. C., Oswald, R., Paasonen, P., Petaja, T., Regelin, E., Sander, R., Sinha, V., Sipila, M., Taraborrelli, D., Ernest, C. T., Williams, J., Lelieveld, J., and Harder, H.: Observation and modelling of HOx radicals in a boreal forest, Atmos. Chem. Phys., 14, 8723-8747, doi:10.5194/acp-14-8723-2014, 2014.

Hosaynali Beygi, Z., Fischer, H., Harder, H. D., Martinez, M., Sander, R., Williams, J., Brookes, D. M., Monks, P. S., and Lelieveld, J.: Oxidation photochemistry in the Southern Atlantic boundary layer: unexpected deviations of photochemical steady state, Atmos. Chem. Phys., 11, 8497-8513, doi:doi:10.5194/acp-11-8497-2011, 2011.

Hu, J., and Stedman, D. H.: Atmospheric RO(X) radicals at an urban site - comparison to a simple theoretical-model, Env. Sci. Tech., 29, 1655-1659, 1995.

Ito, A., Sillman, S., and Penner, J. E.: Effects of additional nonmethane volatile organic compounds, organic nitrates, and direct emissions of oxygenated organic species on global tropospheric chemistry, J. Geophys. Res. -Atmos., 112, doi:10.1029/2005jd006556, 2007.

IUPAC: Task Group on Atmospheric Chemical Kinetic Data Evaluation, (Ammann, M., Cox, R.A., Crowley, J.N., Herrmann, H., Jenkin, M.E., McNeill, V.F., Mellouki, A., Rossi, M. J., Troe, J. and Wallington, T. J.) http://iupac.pole-ether.fr/index.html., 2018.

Jacob, D. J., and Wofsy, S. C.: Photochemistry of biogenic emissions over the Amazon forest, J. Geophys. Res. -Atmos., 93, 1477-1486, doi:10.1029/JD093iD02p01477, 1988.

Jacob, D. J.: Heterogeneous chemistry and tropospheric ozone, Atmos. Env., 34, 2131-2159, doi:10.1016/s1352-2310(99)00462-8, 2000.

Jardine, K. J., Sommer, E. D., Saleska, S. R., Huxman, T. E., Harley, P. C., and Abrell, L.: Gas Phase Measurements of Pyruvic Acid and Its Volatile Metabolites, Env. Sci. Tech., 44, 2454-2460, doi:10.1021/es903544p, 2010.

Jenkin, M. E., Hurley, M. A., and Wallington, T. J.: Investigation of the Radical Product Channel of the CH3OCH2O2 + HO2 Reaction in the Gas Phase, J. Phys. Chem. A, 114, 408-416, doi:10.1021/jp908158w, 2010.

Kawamura, K., Okuzawa, K., Aggarwal, S. G., Irie, H., Kanaya, Y., and Wang, Z.: Determination of gaseous and particulate carbonyls (glycolaldehyde, hydroxyacetone, glyoxal, methylglyoxal, nonanal and decanal) in the atmosphere at Mt. Tai, Atmos. Chem. Phys., 13, 5369-5380, doi:10.5194/acp-13-5369-2013, 2013.

Kim, S., Wolfe, G. M., Mauldin, L., Cantrell, C., Guenther, A., Karl, T., Turnipseed, A., Greenberg, J., Hall, S. R., Ullmann, K., Apel, E., Hornbrook, R., Kajii, Y., Nakashima, Y., Keutsch, F. N., DiGangi, J. P., Henry, S. B., Kaser, L., Schnitzhofer, R., Graus, M., Hansel, A., Zheng, W., and Flocke, F. F.: Evaluation of HOx sources and cycling using measurement-constrained model calculations in a 2-methyl-3-butene-2-ol (MBO) and monoterpene (MT) dominated ecosystem, Atmos. Chem. Phys., 13, 2031-2044, 2013.

Klotz, B., Graedler, F., Sorensen, S., Barnes, I., and Becker, K. H.: A kinetic study of the atmospheric photolysis of alpha-dicarbonyls, Int. J. Chem. Kinet., 33, 9-20, doi:10.1002/1097-4601(20010101)33:1<9::aid-kin2>3.0.co;2-v, 2001.

Kourtchev, I., Giorio, C., Manninen, A., Wilson, E., Mahon, B., Aalto, J., Kajos, M., Venables, D., Ruuskanen, T., Levula, J., Loponen, M., Connors, S., Harris, N., Zhao, D. F., Kiendler-Scharr, A., Mentel, T., Rudich, Y., Hallquist, M., Doussin, J. F., Maenhaut, W., Back, J., Petaja, T., Wenger, J., Kulmala, M., and Kalberer, M.: Enhanced Volatile Organic Compounds emissions and organic aerosol mass increase the oligomer content of atmospheric aerosols, Scientific Reports, 6, 2016.

Kurpius, M. R., and Goldstein, A. H.: Gas-phase chemistry dominates O_3 loss to a forest, implying a source of aerosols and hydroxyl radicals to the atmosphere, Geophys. Res. Lett., 30, doi:10.1029/2002gl016785, 2003.

Lee, Y. N., Zhou, X. L., and Hallock, K.: Atmospheric carbonyl compounds at a rural southeastern United States site, J. Geophys. Res. -Atmos., 100, 25933-25944, doi:10.1029/95jd02605, 1995.

Lelieveld, J., Butler, T. M., Crowley, J. N., Dillon, T. J., Fischer, H., Ganzeveld, L., Harder, H., Lawrence, M. G., Martinez, M., Taraborrelli, D., and Williams, J.: Atmospheric oxidation capacity sustained by a tropical forest, Nature, 452, 737-740, 2008.

Lew, M. M., Dusanter, S., and Stevens, P. S.: Measurement of interferences associated with the detection of the hydroperoxy radical in the atmosphere using laser-induced fluorescence, Atmos. Meas. Tech., 11, 95-109, 2018.

Li, H., Chen, Z. M., Huang, L. B., and Huang, D.: Organic peroxides' gas-particle partitioning and rapid heterogeneous decomposition on secondary organic aerosol, Atmos. Chem. Phys., 16, 1837-1848, doi:10.5194/acp-16-1837-2016, 2016.

Liang, H., Chen, Z. M., Huang, D., Zhao, Y., and Li, Z. Y.: Impacts of aerosols on the chemistry of atmospheric trace gases: a case study of peroxides and HO2 radicals, Atmos. Chem. Phys., 13, 11259-11276, doi:10.5194/acp-13-11259-2013, 2013.

Liebmann, J., Karu, E., Sobanski, N., Schuladen, J., Ehn, M., Schallhart, S., Quéléver, L., Hellen, H., Hakola, H., Hoffmann, T., Williams, J., Fischer, H., Lelieveld, J., and Crowley, J. N.: Direct measurement of NO_3 radical reactivity in a boreal forest, Atmos. Chem. Phys., 2018, 3799-3815, doi:10.5194/acp-18-3799-2018, 2018.

Liu, Z., Wang, Y. H., Gu, D. S., Zhao, C., Huey, L. G., Stickel, R., Liao, J., Shao, M., Zhu, T., Zeng, L. M., Liu, S. C., Chang, C. C., Amoroso, A., and Costabile, F.: Evidence of Reactive Aromatics As a Major Source of Peroxy Acetyl Nitrate over China, Env. Sci. Tech., 44, 7017-7022, doi:10.1021/es1007966, 2010.

Muller, M., Anderson, B. E., Beyersdorf, A. J., Crawford, J. H., Diskin, G. S., Eichler, P., Fried, A., Keutsch, F. N., Mikoviny, T., Thornhill, K. L., Walega, J. G., Weinheimer, A. J., Yang, M., Yokelson, R. J., and Wisthaler, A.: In situ measurements and modeling of reactive trace gases in a small biomass burning plume, Atmos. Chem. Phys., 16, 3813-3824, 2016.

Ng, N. L., Brown, S. S., Archibald, A. T., Atlas, E., Cohen, R. C., Crowley, J. N., Day, D. A., Donahue, N. M., Fry, J. L., Fuchs, H., Griffin, R. J., Guzman, M. I., Hermann, H., Hodzic, A., Iinuma, Y., Jimenez, J. L., Kiendler-Scharr, A., Lee, B. H., Luecken, D. J., Mao, J., McLaren, R., Mutzel, A., Osthoff, H. D., Ouyang, B., Picquet-Varrault, B., Platt, U., Pye, H. O. T., Rudich, Y., Schwantes, R. H., Shiraiwa, M., Stutz, J., Thornton, J. A., Tilgner, A., Williams, B. J., and Zaveri, R. A.: Nitrate radicals and biogenic volatile organic compounds: oxidation, mechanisms and organic aerosol, Atmos. Chem. Phys. Discuss., 2016, 1-111, doi:10.5194/acp-2016-734, 2016.

Nguyen, T. B., Crounse, J. D., Teng, A. P., St. Clair, J. M., Paulot, F., Wolfe, G. M., and Wennberg, P. O.: Rapid deposition of oxidized biogenic compounds to a temperate forest, Proceedings of the National Academy of Sciences, 112, E392, 2015.

Nölscher, A. C., Williams, J., Sinha, V., Custer, T., Song, W., Johnson, A. M., Axinte, R., Bozem, H., Fischer, H., Pouvesle, N., Phillips, G., Crowley, J. N., Rantala, P., Rinne, J., Kulmala, M., Gonzales, D., Valverde-Canossa, J., Vogel, A., Hoffmann, T., Ouwersloot, H. G., Vilà-Guerau de Arellano, J., and Lelieveld, J.: Summertime total OH reactivity measurements from boreal forest during HUMPPA-COPEC 2010, Atmos. Chem. Phys., 12, 8257-8270, doi:10.5194/acp-12-8257-2012, 2012.

Novelli, A., Hens, K., Ernest, C. T., Kubistin, D., Regelin, E., Elste, T., Plass-Duelmer, C., Martinez, M., Lelieveld, J., and Harder, H.: Characterisation of an inlet pre-injector laser-induced fluorescence instrument for the measurement of atmospheric hydroxyl radicals, Atmos. Meas. Tech., 7, 3413-3430, doi:10.5194/amt-7-3413-2014, 2014.

Obermeyer, G., Aschmann, S. M., Atkinson, R., and Arey, J.: Carbonyl atmospheric reaction products of aromatic hydrocarbons in ambient air, Atmos. Env., 43, 3736-3744, doi:10.1016/j.atmosenv.2009.04.015, 2009.

Orlando, J. J., and Tyndall, G. S.: Gas phase UV absorption spectra for peracetic acid, and for acetic acid monomers and dimers, J. Photochem. Photobiol. A-Chem., 157, 161-166, 2003.

5 Ouwersloot, H. G., de Arellano, J. V. G., Nolscher, A. C., Krol, M. C., Ganzeveld, L. N., Breitenberger, C., Mammarella, I., Williams, J., and Lelieveld, J.: Characterization of a boreal convective boundary layer and its impact on atmospheric chemistry during HUMPPA-COPEC-2010, Atmos. Chem. Phys., 12, 9335-9353, doi:10.5194/acp-12-9335-2012, 2012.

Paasonen, P., Asmi, A., Petaja, T., Kajos, M. K., Aijala, M., Junninen, H., Holst, T., Abbatt, J. P. D., Arneth, A., Birmili, W., van der Gon, H. D., Hamed, A., Hoffer, A., Laakso, L., Laaksonen, A., Leaitch, W. R., Plass-Dulmer, C., Pryor, S. C., Raisanen, P., Swietlicki, E.,
10 Wiedensohler, A., Worsnop, D. R., Kerminen, V. M., and Kulmala, M.: Warming-induced increase in aerosol number concentration likely to moderate climate change, Nature Geoscience, 6, 438-442, 2013.

Petäjä, T., Mauldin, R. L., Kosciuch, E., McGrath, J., Nieminen, T., Paasonen, P., Boy, M., Adamov, A., Kotiaho, T., and Kulmala, M.: Sulfuric acid and OH concentrations in a boreal forest site, Atmos. Chem. Phys., 9, 7435-7448, 2009.

Phillips, G. J., Pouvesle, N., Thieser, J., Schuster, G., Axinte, R., Fischer, H., Williams, J., Lelieveld, J., and Crowley, J. N.: Peroxyacetyl
15 nitrate (PAN) and peroxyacetic acid (PAA) measurements by iodide chemical ionisation mass spectrometry: first analysis of results in the boreal forest and implications for the measurement of PAN fluxes, Atmos. Chem. Phys., 13, 1129-1139, doi:doi:10.5194/acp-13-1129-2013, 2013.

Platt, U., Lebras, G., Poulet, G., Burrows, J. P., and Moortgat, G.: Peroxy-radicals from nighttime reactions of NO_3 with organic compounds, Nature, 348, 147-149, 1990.

20 Reiner, T., Hanke, M., and Arnold, F.: Atmospheric peroxy radical measurements by ion molecule reaction mass spectrometry: A novel analytical method using amplifying chemical conversion to sulfuric acid, J. Geophys. Res. -Atmos., 102, 1311-1326, 1997.

Rinne, J., Markkanen, T., Ruuskanen, T. M., Petaja, T., Keronen, P., Tang, M. J., Crowley, J. N., Rannik, U., and Vesala, T.: Effect of chemical degradation on fluxes of reactive compounds –a study with a stochastic Lagrangian transport model, Atmos. Chem. Phys., 12, 4843-4854, 2012.

25 Roberts, J. M.: The atmospheric chemistry of organic nitrates, Atmos. Environ., Part A, 24, 243-287, doi:doi:10.1016/0960-1686(90)90108-y, 1990.

Rypkema, H. A., and Francisco, J. S.: Atmospheric Oxidation of Peroxyacetic Acid, J. Phys. Chem. A, 117, 14151-14162, 2013.

Salisbury, G., Rickard, A. R., Monks, P. S., Allan, B. J., Bauguitte, S., Penkett, S. A., Carslaw, N., Lewis, A. C., Creasey, D. J., Heard, D. E., Jacobs, P. J., and Lee, J. D.: Production of peroxy radicals at night via reactions of ozone and the nitrate radical in the marine boundary
30 layer, J. Geophys. Res. -Atmos., 106, 12669-12687, 2001.

Schade, G. W., Goldstein, A. H., Gray, D. W., and Lerdau, M. T.: Canopy and leaf level 2-methyl-3-buten-2-ol fluxes from a ponderosa pine plantation, Atmos. Env., 34, 3535-3544, doi:10.1016/s1352-2310(00)00120-5, 2000.

Shepson, P. B., Bottenheim, J. W., Hastie, D. R., and Venkatram, A.: DETERMINATION OF THE RELATIVE OZONE AND PAN DEPOSITION VELOCITIES AT NIGHT, Geophys. Res. Lett., 19, 1121-1124, doi:10.1029/92gl01118, 1992.

35 Singh, H. B., and Hanst, P. L.: Peroxyacetyl nitrate (PAN) in the unpolluted atmosphere: An important reservoir for nitrogen oxides, Geophys. Res. Lett., 8, 941-944, 1981.

Singh, H. B.: REACTIVE NITROGEN IN THE TROPOSPHERE, Env. Sci. Tech., 21, 320-327, 1987.

Sommariva, R., Bates, T. S., Bon, D., Brookes, D. M., de Gouw, J. A., Gilman, J. B., Herndon, S. C., Kuster, W. C., Lerner, B. M., Monks, P. S., Osthoff, H. D., Parker, A. E., Roberts, J. M., Tucker, S. C., Warneke, C., Williams, E. J., Zahniser, M. S., and Brown, S. S.:
40 Modelled and measured concentrations of peroxy radicals and nitrate radical in the US Gulf Coast region during TexAQS 2006, J. Atmos. Chem., 68, 331-362, 2011.

Sparks, J. P., Roberts, J. M., and Monson, R. K.: The uptake of gaseous organic nitrogen by leaves: A significant global nitrogen transfer process, Geophys. Res. Lett., 30, doi:10.1029/2003gl018578, 2003.

Spaulding, R. S., Schade, G. W., Goldstein, A. H., and Charles, M. J.: Characterization of secondary atmospheric photooxidation products:
45 Evidence for biogenic and anthropogenic sources, J. Geophys. Res. -Atmos., 108, doi:10.1029/2002jd002478, 2003.

Stickler, A., Fischer, H., Williams, J., de Reus, M., Sander, R., Lawrence, M. G., Crowley, J. N., and Lelieveld, J.: Influence of summertime deep convection on formaldehyde in the middle and upper troposphere over Europe, J. Geophys. Res. -Atmos., 111, D14308, doi:10.1029/2005JD007001, 2006.

Stickler, A., Fischer, H., Bozem, H., Gurk, C., Schiller, C., Martinez-Harder, M., Kubistin, D., Harder, H., Williams, J., Eerdekens, G.,
50 Yassaa, N., Ganzeveld, L., Sander, R., and Lelieveld, J.: Chemistry, transport and dry deposition of trace gases in the boundary layer over the tropical Atlantic Ocean and the Guyanas during the GABRIEL field campaign, Atmos. Chem. Phys., 7, 3933-3956, 2007.

Stockwell, C. E., Veres, P. R., Williams, J., and Yokelson, R. J.: Characterization of biomass burning emissions from cooking fires, peat, crop residue, and other fuels with high-resolution proton-transfer-reaction time-of-flight mass spectrometry, Atmos. Chem. Phys., 15, 845-865, doi:10.5194/acp-15-845-2015, 2015.

55 Stoenner, C., Derstroff, B., Klupfel, T., Crowley, J. N., and Williams, J.: Glyoxal measurement with a proton transfer reaction time of flight mass spectrometer (PTR-TOF-MS): characterization and calibration, J. Mass Spectrom., 52, 30-35, doi:10.1002/jms.3893, 2017.

Talbot, R. W., Beecher, K. M., Harriss, R. C., and Cofer, W. R.: Atmospheic geochemistry of formic and acetic-acids at a mod-latitude temperate site J. Geophys. Res. -Atmos., 93, 1638-1652, doi:10.1029/JD093iD02p01638, 1988.

Talbot, R. W., Mosher, B. W., Heikes, B. G., Jacob, D. J., Munger, J. W., Daube, B. C., Keene, W. C., Maben, J. R., and Artz, R. S.: Carboxylic acids in the rural continental atmosphere over the eastern United States during the Shenandoah Cloud and Photochemistry Experiment, Journal of Geophysical Research: Atmospheres, 100, 9335-9343, doi:10.1029/95jd00507, 1995.

Talukdar, R. K., Burkholder, J. B., Schmoltner, A. M., Roberts, J. M., Wilson, R. R., and Ravishankara, A. R.: Investigation of the loss processes for peroxyacetyl nitrate in the atmosphere: UV photolysis and reaction with OH, J. Geophys. Res. -Atmos., 100, 14163-14173, doi:doi:10.1029/95jd00545, 1995.

Tan, Y., Lim, Y. B., Altieri, K. E., Seitzinger, S. P., and Turpin, B. J.: Mechanisms leading to oligomers and SOA through aqueous photooxidation: insights from OH radical oxidation of acetic acid and methylglyoxal, Atmos. Chem. Phys., 12, 801-813, doi:10.5194/acp-12-801-2012, 2012.

Taraborrelli, D., Lawrence, M. G., Crowley, J. N., Dillon, T. J., Gromov, S., Groß, C. B. M., Vereecken, L., and Lelieveld, J.: Hydroxyl radical buffered by isoprene oxidation over tropical forests, Nature Geoscience, 5, 190-193, 2012.

Thornton, J. A., Jaegle, L., and McNeill, V. F.: Assessing known pathways for HO2 loss in aqueous atmospheric aerosols: Regional and global impacts on tropospheric oxidants, J. Geophys. Res. -Atmos., 113, doi:10.1029/2007jd009236, 2008.

Turnipseed, A. A., Huey, L. G., Nemitz, E., Stickel, R., Higgs, J., Tanner, D. J., Slusher, D. L., Sparks, J. P., Flocke, F., and Guenther, A.: Eddy covariance fluxes of peroxyacetyl nitrates (PANs) and NOy to a coniferous forest, J. Geophys. Res. -Atmos., 111, D09304, 2006.

Tyndall, G. S., Cox, R. A., Granier, C., Lesclaux, R., Moortgat, G. K., Pilling, M. J., Ravishankara, A. R., and Wallington, T. J.: Atmospheric chemistry of small organic peroxy radicals, J. Geophys. Res. -Atmos., 106, 12157-12182, doi:10.1029/2000jd900746, 2001.

Veres, P. R., Roberts, J. M., Cochran, A. K., Gilman, J. B., Kuster, W. C., Holloway, J. S., Graus, M., Flynn, J., Lefer, B., Warneke, C., and de Gouw, J.: Evidence of rapid production of organic acids in an urban air mass, Geophys. Res. Lett., 38, doi:10.1029/2011gl048420, 2011.

Volkamer, R., Platt, U., and Wirtz, K.: Primary and secondary glyoxal formation from aromatics: Experimental evidence for the bicycloalkyl-radical pathway from benzene, toluene, and p-xylene, J. Phys. Chem. A, 105, 7865-7874, doi:doi:10.1021/jp010152w, 2001.

Williams, J., Roberts, J. M., Fehsenfeld, F. C., Bertman, S. B., Buhr, M. P., Goldan, P. D., Hubler, G., Kuster, W. C., Ryerson, T. B., Trainer, M., and Young, V.: Regional ozone from biogenic hydrocarbons deduced from airborne measurements of PAN, PPN, and MPAN, Geophys. Res. Lett., 24, 1099-1102, 1997.

Williams, J., Crowley, J., Fischer, H., Harder, H., Martinez, M., Petaja, T., Rinne, J., Back, J., Boy, M., Dal Maso, M., Hakala, J., Kajos, M., Keronen, P., Rantala, P., Aalto, J., Aaltonen, H., Paatero, J., Vesala, T., Hakola, H., Levula, J., Pohja, T., Herrmann, F., Auld, J., Mesarchaki, E., Song, W., Yassaa, N., Nolscher, A., Johnson, A. M., Custer, T., Sinha, V., Thieser, J., Pouvesle, N., Taraborrelli, D., Tang, M. J., Bozem, H., Hosaynali-Beygi, Z., Axinte, R., Oswald, R., Novelli, A., Kubistin, D., Hens, K., Javed, U., Trawny, K., Breitenberger, C., Hidalgo, P. J., Ebben, C. J., Geiger, F. M., Corrigan, A. L., Russell, L. M., Ouwersloot, H. G., de Arellano, J. V. G., Ganzeveld, L., Vogel, A., Beck, M., Bayerle, A., Kampf, C. J., Bertelmann, M., Kollner, F., Hoffmann, T., Valverde, J., Gonzalez, D., Riekkola, M. L., Kulmala, M., and Lelieveld, J.: The summertime Boreal forest field measurement intensive (HUMPPA-COPEC-2010): an overview of meteorological and chemical influences, Atmos. Chem. Phys., 11, 10599-10618, doi:10.5194/acp-11-10599-2011, 2011.

Wolfe, G. M., Thornton, J. A., Yatavelli, R. L. N., McKay, M., Goldstein, A. H., LaFranchi, B., Min, K. E., and Cohen, R. C.: Eddy covariance fluxes of acyl peroxy nitrates (PAN, PPN and MPAN) above a Ponderosa pine forest, Atmos. Chem. Phys., 9, 615-634, 2009.

Wu, H., Wang, Y., Li, H., Huang, L., Huang, D., Shen, H., Xing, Y., and Chen, Z.: The OH-initiated oxidation of atmospheric peroxyacetic acid: Experimental and model studies, Atmos. Env., 164, 61-70, 2017.

Wu, Q. Q., Huang, L. B., Liang, H., Zhao, Y., Huang, D., and Chen, Z. M.: Heterogeneous reaction of peroxyacetic acid and hydrogen peroxide on ambient aerosol particles under dry and humid conditions: kinetics, mechanism and implications, Atmos. Chem. Phys., 15, 6851-6866, 2015.

Yanez-Serrano, A. M., Nolscher, A. C., Bourtsoukidis, E., Derstroff, B., Zannoni, N., Gros, V., Lanza, M., Brito, J., Noe, S. M., House, E., Hewitt, C. N., Langford, B., Nemitz, E., Behrendt, T., Williams, J., Artaxo, P., Andreae, M. O., and Kesselmeier, J.: Atmospheric mixing ratios of methyl ethyl ketone (2-butanone) in tropical, boreal, temperate and marine environments, Atmos. Chem. Phys., 16, 10965-10984, 2016.

Yassaa, N., Song, W., Lelieveld, J., Vanhatalo, A., Back, J., and Williams, J.: Diel cycles of isoprenoids in the emissions of Norway spruce, four Scots pine chemotypes, and in Boreal forest ambient air during HUMPPA-COPEC-2010, Atmos. Chem. Phys., 12, 7215-7229, doi:10.5194/acp-12-7215-2012, 2012.

Yu, J. Z., Flagan, R. C., and Seinfeld, J. H.: Identification of products containing -COOH, -OH, and -C=O in atmospheric oxidation of hydrocarbons, Env. Sci. Tech., 32, 2357-2370, doi:10.1021/es980129x, 1998.

Zhang, L., Jacob, D. J., Boersma, K. F., Jaffe, D. A., Olson, J. R., Bowman, K. W., Worden, J. R., Thompson, A. M., Avery, M. A., Cohen, R. C., Dibb, J. E., Flock, F. M., Fuelberg, H. E., Huey, L. G., McMillan, W. W., Singh, H. B., and Weinheimer, A. J.: Transpacific transport of ozone pollution and the effect of recent Asian emission increases on air quality in North America: an integrated analysis using satellite, aircraft, ozonesonde, and surface observations, Atmos. Chem. Phys., 8, 6117-6136, 2008.

Zhang, X., Chen, Z. M., He, S. Z., Hua, W., Zhao, Y., and Li, J. L.: Peroxyacetic acid in urban and rural atmosphere: concentration, feedback on PAN-NO(x) cycle and implication on radical chemistry, Atmos. Chem. Phys., 10, 737-748, 2010.

5   Acknowledgements

We thank Uwe Parchatka and Markus Rudolf as well as the technical staff of SMEAR II station for technical support during HUMPPA-COPEC-2010. Funding from Academy of Finland via Center of Excellence in Atmospheric Science and European Commission via ACTRIS-2 is gratefully acknowledged.
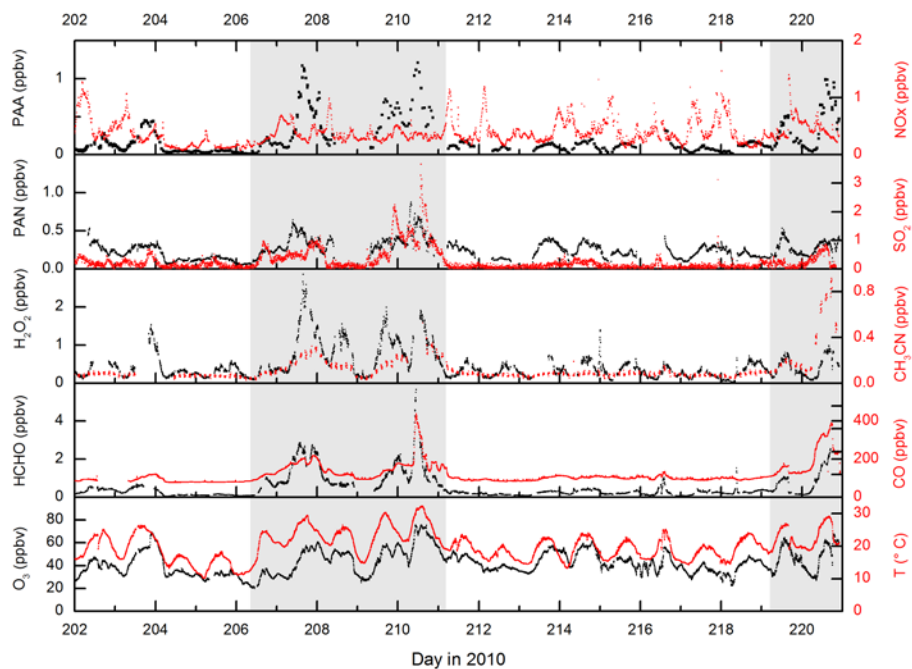
Figure 1: Measurements of PAA (CH₃C(O)OOH), PAN (CH₃C(O)O₂NO₂) and other trace gases during HUMPPA-COPEC-2010. Day 202 was the 20th July, 2010. The shaded areas represent two periods in which the site was impacted by biomass-burning plumes originating from Russia.
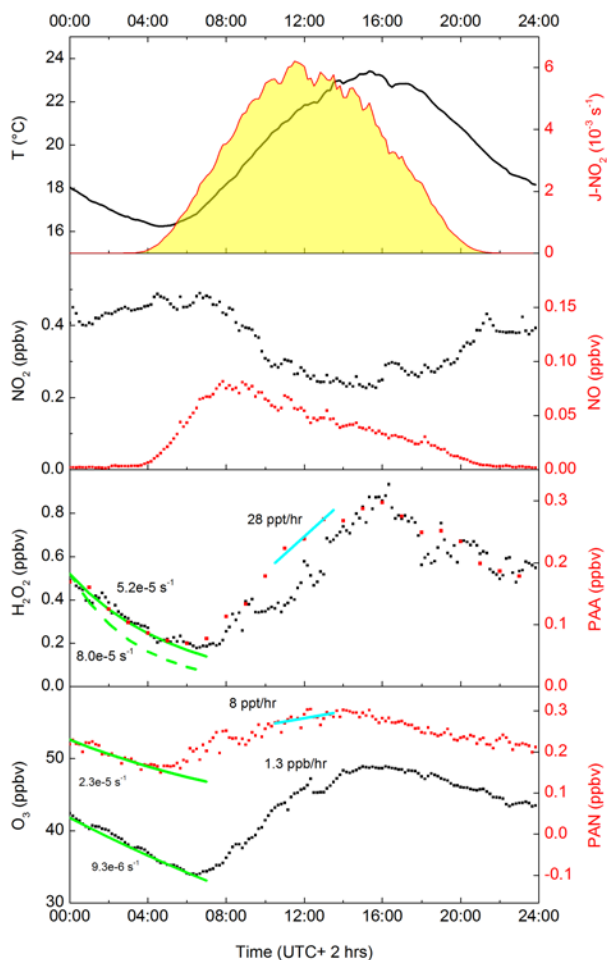
Figure 2: Averaged diel profiles (day 202-220) of PAN, O₃, H₂O₂, NO₂, NO, temperature, J-O(¹D) (all 10 min averages) and PAA (60 min intervals). The solid green lines represent campaign averaged, nighttime exponential decay rate constants (s⁻¹) for H₂O₂, PAA, PAN and O₃. The dashed green line is the adjusted decay constant for H₂O₂ that takes its formation via ozonolysis of VOCs into account. The cyan lines represent average, production rates (ppbv or pptv per hour) for PAA and PAN (centred at 12:00).
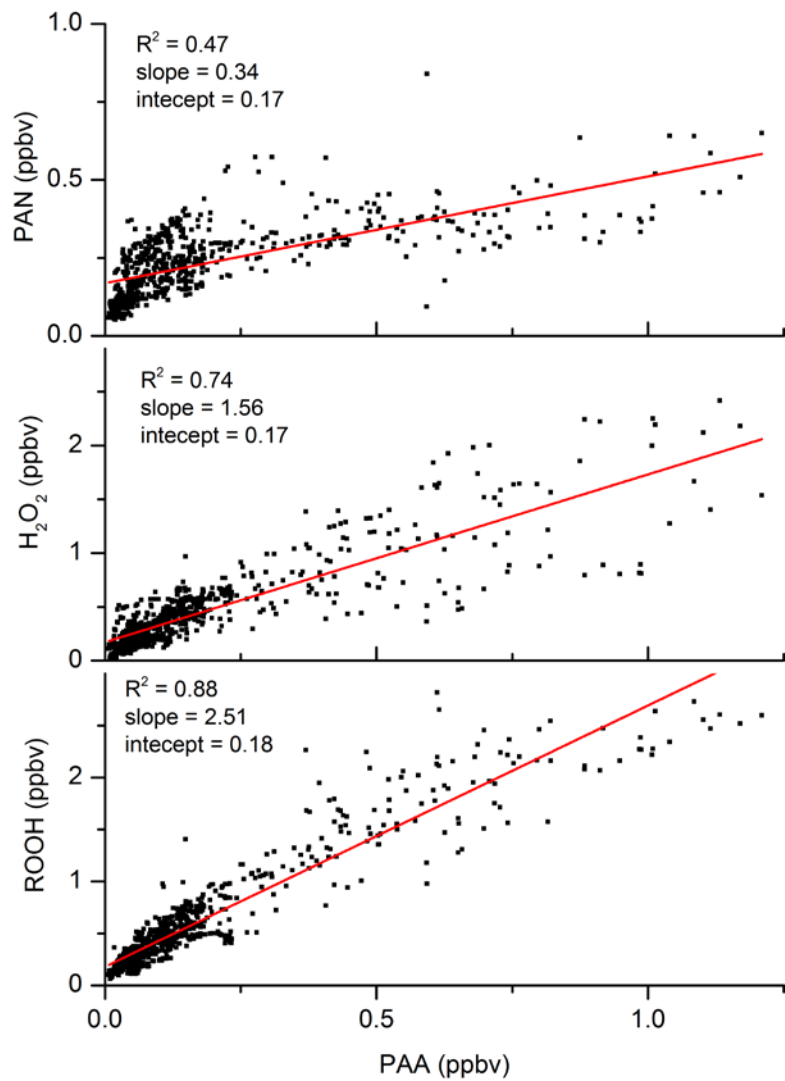
Figure 3: Correlation of PAA with PAN, H$_2$O$_2$ and ROOH (total organic peroxides).
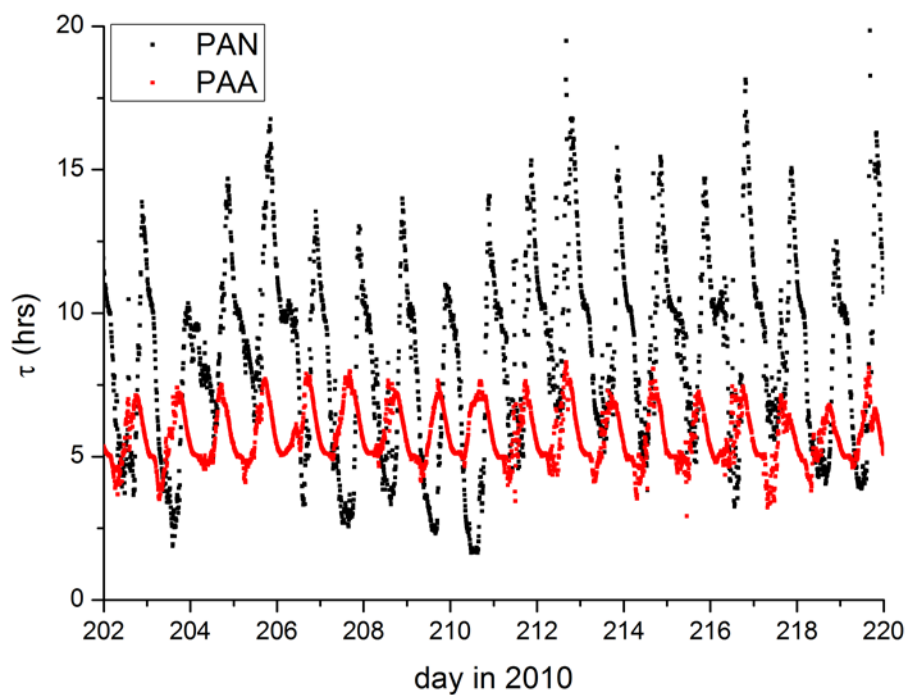
Figure 4: **Lifetimes of PAN and PAA. The more regular diel cycle of PAA reflects the dominance of dry deposition with only a small contribution due to OH (visible as some fine structure in the midday loss rate constant). PAN losses are dominated by thermal decomposition during the day and deposition at night.**
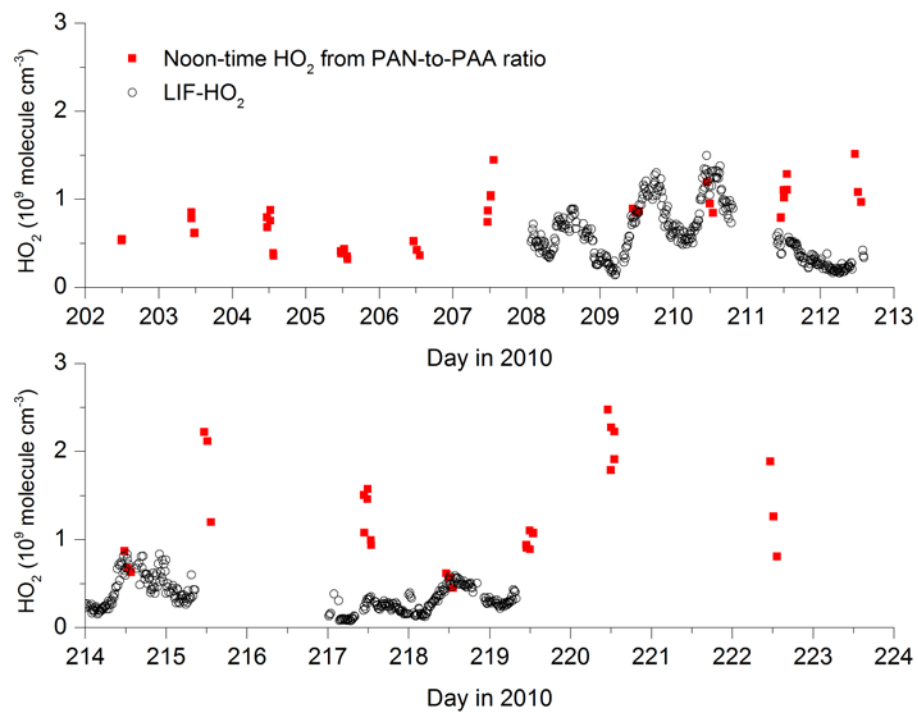
Figure 5: [HO₂] calculated via the PAN-to-PAA ratio at local noon (red symbols) and comparison with measured HO₂ (black data-points) by LIF-FAGE.
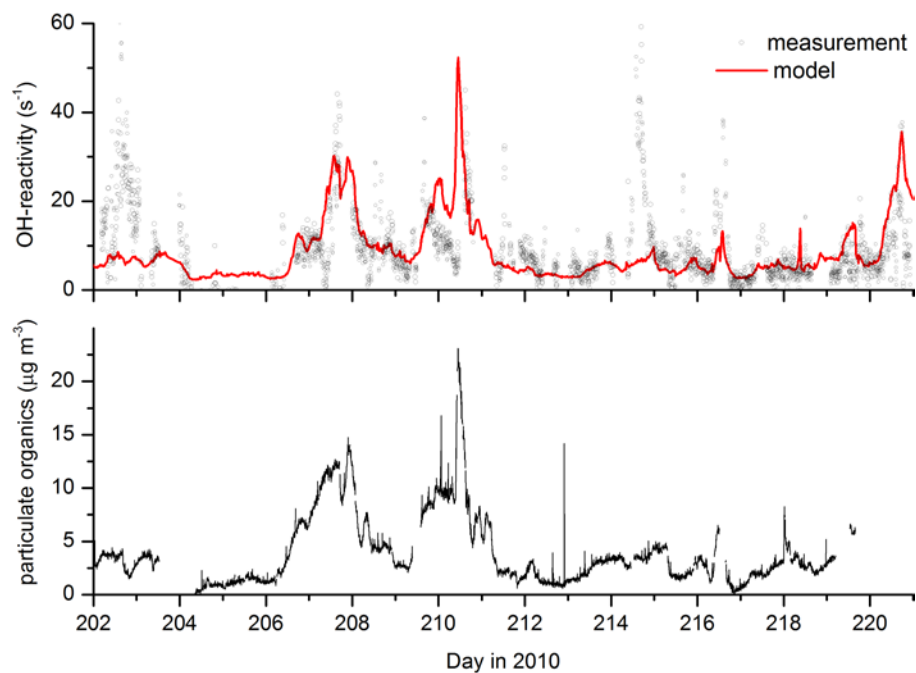
Figure 6: Upper panel: Measured (black data-points) and modelled OH reactivity (red line). The aerosol organic content (lower panel) shows similar campaign variability to modelled OH-reactivity.
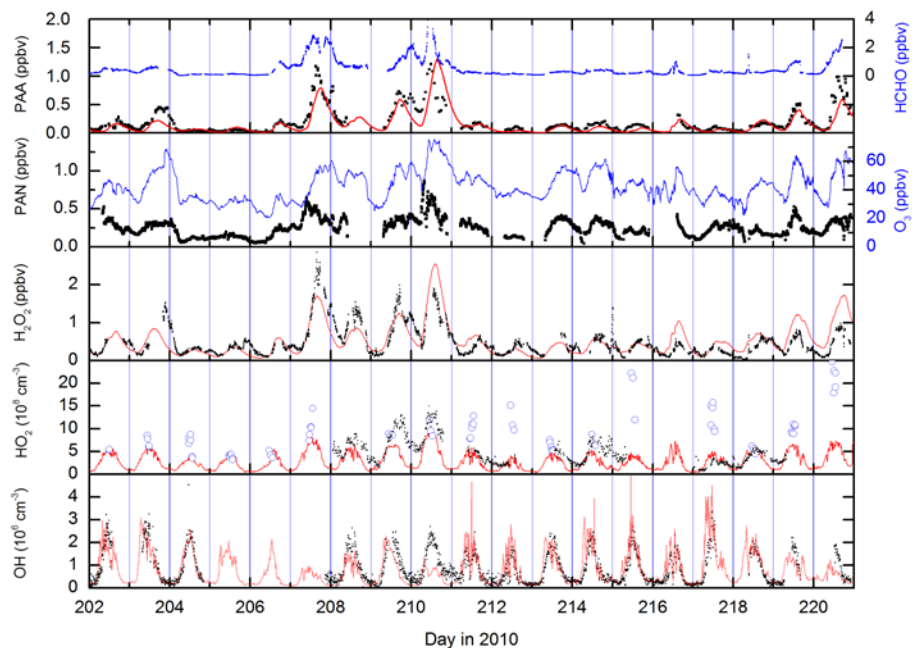
Figure 7: Measurements (black and blue data-points) and model (red lines). The OH dataset displayed is from CIMS measurements at ground level and has been adjusted to match levels observed at canopy height (see supplementary information and Hens et al., 2014). The open, violet circles are HO$_2$ concentrations calculated from the PAN-to-PAA ratio and the steady-state expression (eqn. 4) presented in section 3.1.
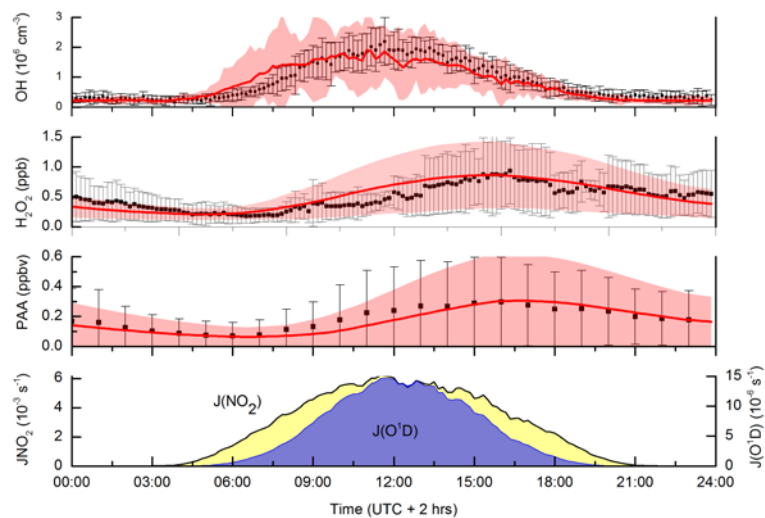
Figure 8: Campaign averaged (days 202 to 220) diel profiles of OH, PAA and H$_2$O$_2$. Measurements are black data-points, error bars are 1σ variability. Model results are the red lines with the shaded area representing 1σ variability. The diel averaged photolysis rate constants of NO$_2$ and O(^{1}D) are displayed as indicators of photochemical activity.
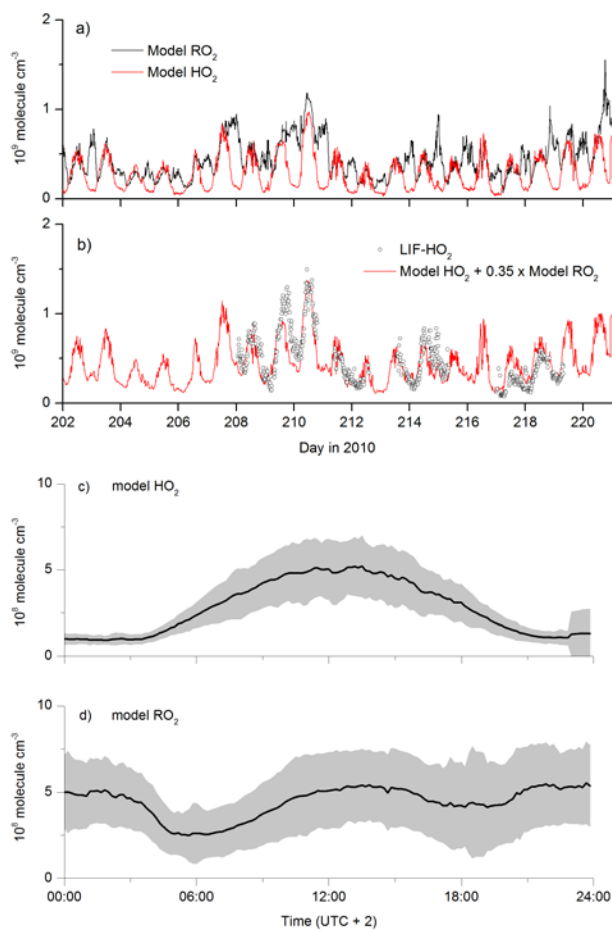
Figure 9: Modelled HO$_2$ and RO$_2$ concentrations as time series (a) and campaign averaged diel profiles (c and d). RO$_2$* represents organic peroxy radicals formed in the OH-initiated degradation of OVOCs and terpenes. The red line in plot (b) is the sum of model HO$_2$ concentration plus 0.35 times the model RO$_2$ concentration.
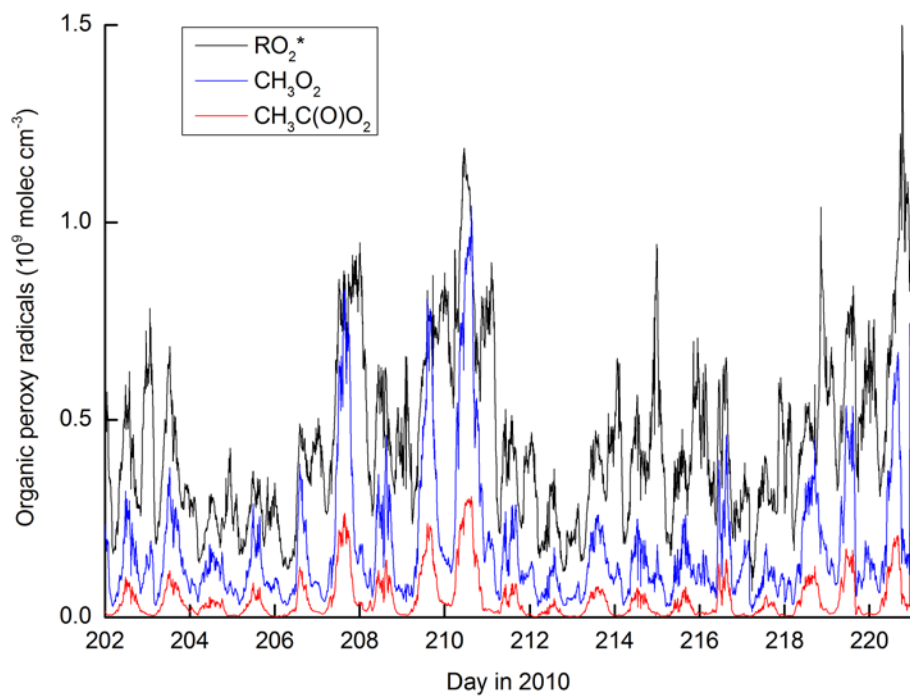
Figure 10: Modelled organic peroxy radical concentrations. RO$_2$* represents organic peroxy radicals formed in the OH-initiated degradation of OVOCs and terpenes.
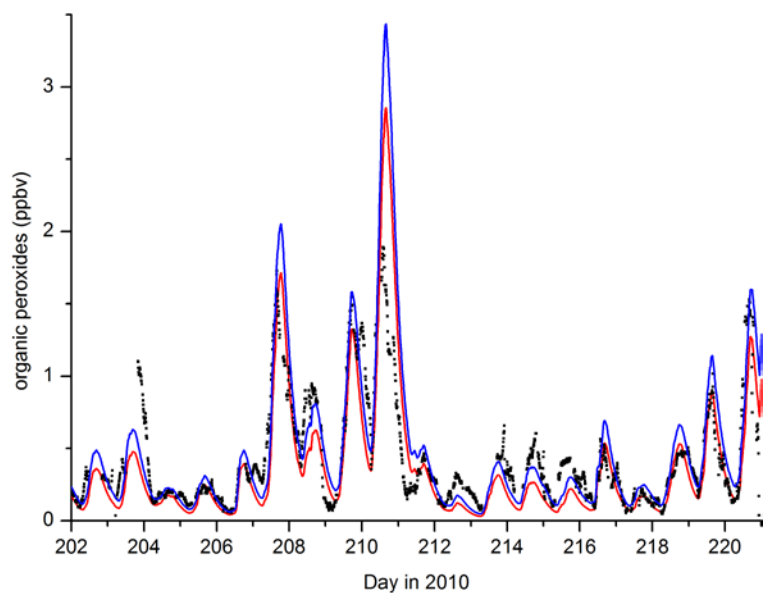
Figure 11: Total organic peroxide measurement (black data-points) and model results. The red line is the modelled sum of CH$_3$OOH and PAA, the blue line includes a contribution (10%) from model ROOH which is formed from RO$_2$* + HO$_2$.
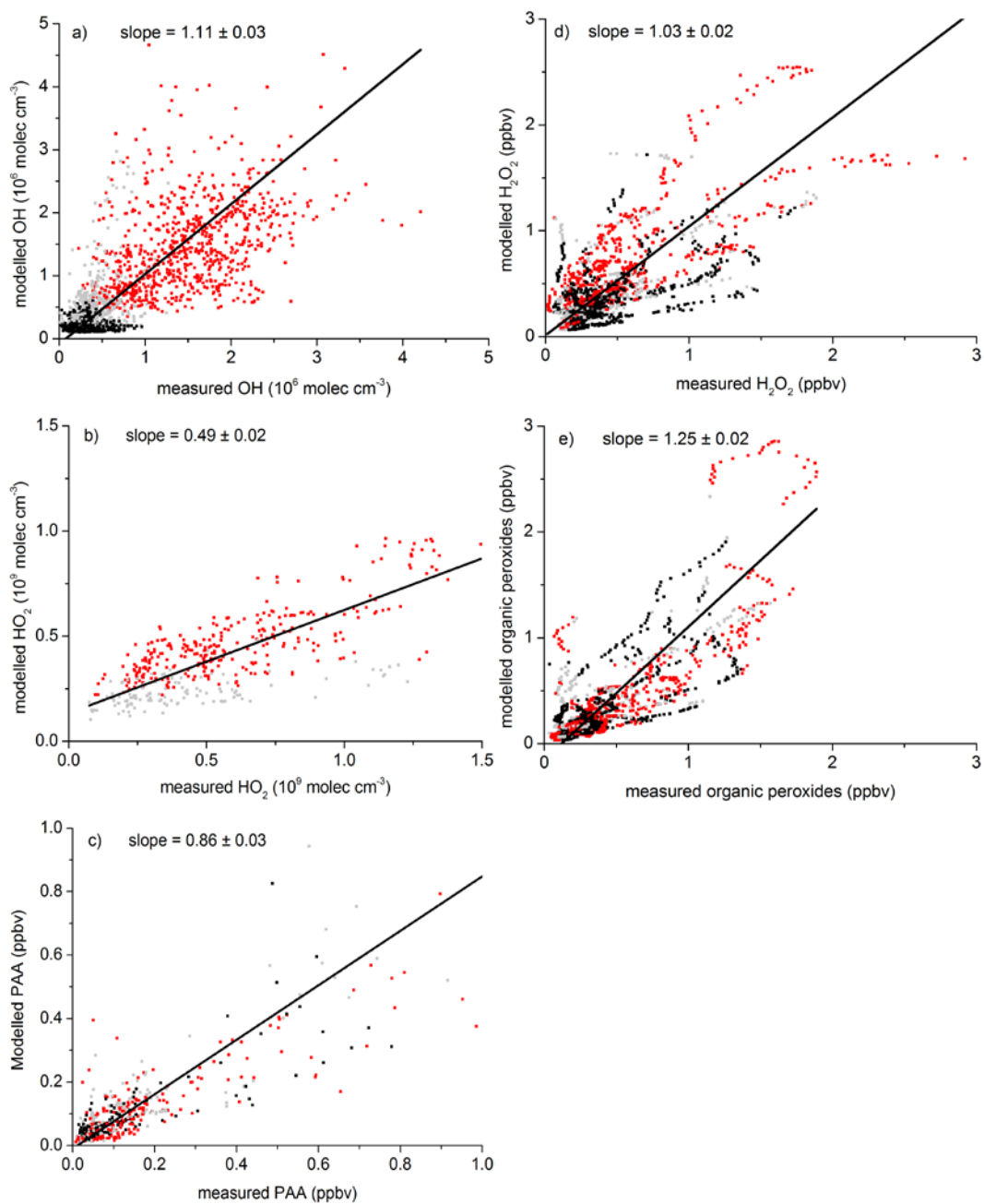
Figure 12: Measurement versus model results for OH, HO₂, (HO₂*), H₂O₂, PAA and ROOH. Red data are daytime, black and grey are dusk and nighttime. The fit lines account for uncertainty in both axes. Uncertainty is statistical (1σ).
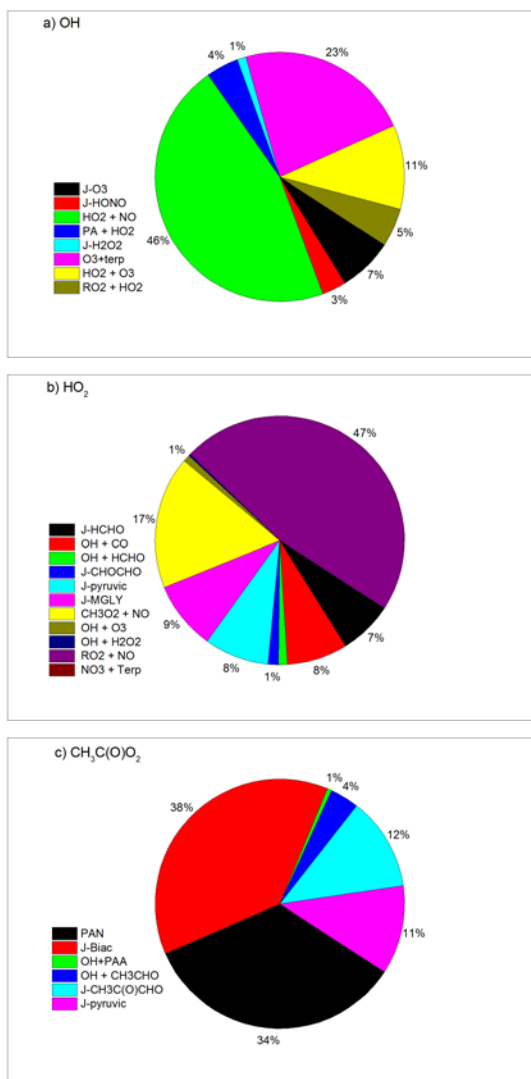
Figure 13. Modelled relative sources (throughout the diel cycle) of OH, HO₂ and CH₃C(O)O₂ during HUMPPA-COPEC-2010 (days 202-220).